1998

Relationship between chemical composition and film properties of organic spin-on glass

Hsiu-Hung Kuo
Lehigh University

Kuo, Hsiu-Hung

Relationship Between Chemical Composition and Film Properties of Organic...

January 11, 1998

Relationship between Chemical Composition and Film Properties of Organic Spin-on Glass

by

Hsiu-Hung Kuo

A Thesis

Presented to the Graduate and Researh Committee

of Lehigh University

in Candidacy for the Degree of

Master of Science

in

Materials Science and Engineering

Lehigh University

May 1996

Certicate of approval

This thesis is accepted and approved in partial fulfillment of the requirements for the degree of Master of Science.

June 21, 1996

Date

Thesis Adviser

Co-Adviser

Chairperson of Department

Acknowledgements

I would like to thank my advisor Dr. Dennis W. Hess and my co-advisor Dr. Manoj K. Chaudhuny for their guidances and assistances on this project. In addition, I would like to extend my thanks to Dr. Qiang Zhao, Sita R. kaluri, Kristine Albrecht, and Bin-Ming Chaung Newby for their kindness helps and useful discussions in this project.

Table of Contents

List of Table

Table of Figure

Abstract

This thesis describes the characterization of thin Spin on Glass (SOG) films used in Complementary Metal Oxide Semiconductor (CMOS) devices, integrated circuits (ICs), and flat panel displays (FPDs). Film thickness as a function of final speed and solution concentration is studied. Higher final speed decreases the film thickness at the same solution concentration, while higher concentration solutions increase the film thickness at a fixed spin speed. Film composition changes are identified by Fourier Transform Infrared Spectroscopy (FTIR) and X-ray photoelectron spectroscopy (XPS) under different annealing temperatures (200-1000^{0}C) and ambients (air, nitrogen, nitrogen with saturated water vapor, oxygen with saturated water vapor, oxygen). Both FTIR and XPS indicate that densification of SOG takes place at anneal temperatures above 600^{0}C. Silicon substrate oxidation occurs above a temperature of 800^{0}C. As the anneal temperature increases, the bonding structure of Si-O changes from Si-O-Si symmetric stretching to asymmetric Si-O stretching and the silanol (Si-OH) bonding changes from hydrogen bonding (or H-bonded water) silanol to isolated silanol bonding. Silanol bonding is eliminated above a temperature of 800^{0}C. In addition, the carbon and nitrogen content in the film decreases as the temperature increases from 200-1000^{0}C.

Oxygen plasma treatment also changes the film bonding environment

as measured by FTIR. An oxygen plasma anodization treatment at 250^{0}C has almost the same effect on film refractive index as that of a thermal treatment at 800^{0}C or higher. Samples annealed at lower temperatures have a higher carbon content which results in a lower wet etching depth in dilute HF (1:500=HF: NH_4F). In contrast, the etching depth by reactive ion etching (RIE) is higher for the lower temperature annealed samples, since porosity is higher. The surface morphogy of SOG films after O_2 reactive ion etching is smooth for 600^{0}C and 1000^{0}C annealed samples. Surfaces of films are rough after an O_2/CHF_3 reactive ion etching treatment due to film attack by fluoride atoms. The 400^{0}C annealed SOG film has a lower dielectric constant than the 600^{0}C annealed SOG film. Capacitance -Voltage plots of 400^{0}C annealed films show hysteresis due to large polarization instabilities related to silanol (Si-OH) while 600^{0}C annealed films display carrier trapping.

Chapter 1

Introduction

1.1 Spin Coating

A key component in the successful production of flat panel displays (FPDs) and integrated circuits (ICs) is proper creation of thin films. These films must be uniformly thin, homogeneous and free of particle defects. Spin coating is a mature technique involving the acceleration of a liquid puddle on a rotating substrate. The process involves a balance between centrifugal forces and viscous forces. Centrifugal forces are controlled by spin speed and acceleration, while viscous forces are determined by solvent viscosity, solvent evaporation rate, and the solids content of the precursor. Recently, spin coating has been used widely in the formation of thin organic films in the fabrication of flat panel display (FPDs) and integrated circuits (ICs). In this process, a fixed amount of polymer solution is dispensed onto a wafer, and the wafer accelerated to a constant spin speed. During the spinning, polymer solution flow across the wafer and solvent evaporates, ultimately forming a solid film.

Von Karman[1] was the first person to propose a mathematical analysis to verify that the film thins and can become more uniform as the spin process proceeds. Emslie et al.[2] showed that for a Newtonian fluid (linear

with topology. The model predicts that for a given coating thickness, step height is not sensitive to initial concentration, spin speed, or radial position. Coating profile is determined by the balance of centrifugal forces, capillary forces, and viscosity forces. In the case of high polymer concentration, the diffusion coefficient decreased exponentially as the solvent concentration decreased. This corresponds to a transition in drying from evaporation control to diffusion control.

Other experiments indicated that as the angular speed increases, the film thickness decreases.[14-17] For a given speed, the film thickness decreases rapidly at first, and then slows down at longer time. The final film thickness is proportional to the solid concentration of fluid, because the viscosity has increased.[14-17]

1.2 Spin on Glass (SOG) Application for ULSI (Ultra Large Scale Integration) Technology

Silicon- containing dielectric films are used widely in microelectronic devices and integrated circuits (ICs). Dielectrics are important components in the structure of CMOS (Complimentary Metal Oxide Semiconductor) devices. These films are currently used as passivation layers, interlevel dielectrics (ILD) or intermetal dielectrics (IMD) , field isolation layers and gate oxides. Several techniques have been used to grow or form dielectric thin

relationship between shear stress and shear rate), the thickness decreases continuously as material is thrown from the wafer. Acrivos et al.[3] extended such analyses to non-Newtonian liquids and showed that the film no longer approached a uniform- thickness condition. Flack et al.[4] modeled the spinning of non- Newtonian solutions by describing the two major film thickness reduction mechanisms: convection due to radial flow and mass transport by solvent evaporation. Convection dominates at the early stages in the process, while solvent evaporation becomes significant towards the end. These model predictions agreed well with experimental observations that the film thickness and uniformity are strong functions of the solution viscosity, the final spin speed and the spin acceleration characteristics. In addition, White[5] has investigated the planarization over isolated lines. Wilson et al.[6] reported planarization of dense topographic features. Bornside[7-9] studied coating on topology and published a two dimensional drying and leveling model. Stillwagon[10] et al. evaluated an epoxy film (non-volatile liquid) profile cured during spinning. LaVergne et al.[11] suggested that the dry coating step height could be approximated by considering only shrinkage from flat wet coating and not considering the effect of centrifugal force and capillary force. Sukanek[12] modeled coating at sindsoidal surfaces and considered Overdiep's leveling mechanism. Gu[13] et al. modeled spin coating of a polymer film on a substrate

films. For example, chemically vapor deposited (CVD) SiO_2 layers from tetraethoxysilane (TEOS) have been used for many years [18-20], while RF biased high density plasma CVD methods [21] have been developed recently. In these technologies, many problems still remain , such as step coverage, particle generation , process reliability, cost considerations, and gap filling capability. The SOG (Spin on glass) process is considered the simplest process that can satisfy both good gap filling and planarization capability. Spin on glass materials consist of Si-O network polymers dissolved in common organic solvents, such as alcohols, ketones, and esters. The oxygen and silicon containing compounds undergo hydrolysis -condensation reactions to form polymer like layers that pyrolyze at relatively high temperatures to form an inorganic glass.

There are several kinds of SOG materials used currently in the semiconductor industry; silicate (or silanol) and polysiloxane polymers are two of the most common. The major difference between a silicate glass and a siloxane material is that there are no organic groups in the silicate materials. The polymer arrangement in a silicate enables the silicon groups to bond to hydroxyl groups (OH), thereby allowing water to be absorbed into the film.[22] Previous studies have shown that dielectric constants for silicate materials are higher than siloxanes because of moisture in the glass.[23,24]

Different kinds of molecular structuresfor the galss described above are shown in Fig 1.1.[25] The chemistry of the proto-typical reaction can be described by the hydrolysis- condensation reaction sequence of tetraethoxysilane(TEOS), $Si(OEt)_4$:

Hydrolysis: $Si(OEt)_4 + H_2O \text{-------} > EtOH + Si(OEt)_3 OH$ or $Si(OEt)_2(OH)_2$,

Condensation: $\equiv SiOH + OHSi\equiv \text{--------} > \equiv Si\text{-}O\text{-}Si\equiv + H_2O$

The properties of SOG materials can be modified by incorporating a substituted alkoxysilane, $RSi(OEt)_3$ where R=methyl or phenyl for $Si(OEt)_4$, or by doping with phosphorous- or boron-containing compounds during the hydrolysis reaction [26].

1.3 Oxygen (O_2) Plasma Conversion of SOG materials

Plasma are used widely in the manufacture of ICs and FPDs, specially, they find use in sputtering[27], plasma enhanced chemical vapor deposition (PECVD)[28] , plasma etching[29], reactive ion etching [30] (RIE), and ion sources for the ion implantation.[31] A plasma can be thought of as a collection of electrons, singly and multiply charged positive and negative ions along with neutral atoms, molecules, and molecular fragments. [32,33] Plasma are formed by the application of an low pressure gas. In this environment, the resulting electric field to a electrons are not in thermal equilibrium with the gas molecules or the ions. Electrons and gas molecules have different

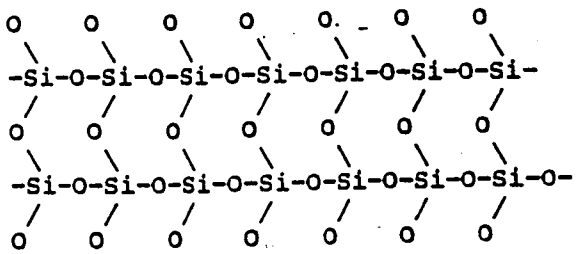

a. Silicate SOG

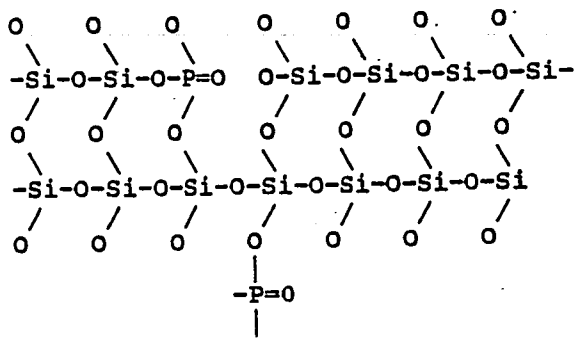

b. P-doped silicate SOG

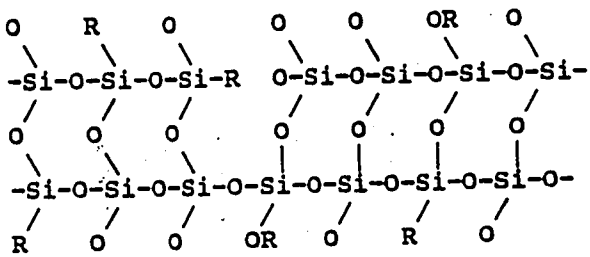

c. Siloxane SOG

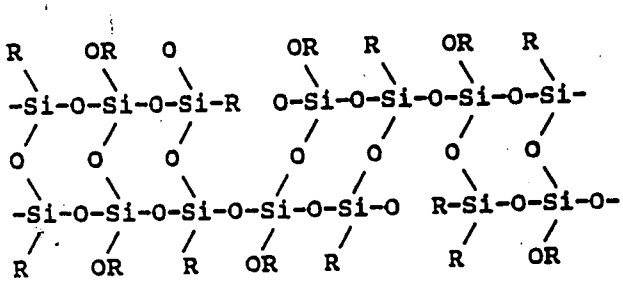

d. High organic siloxane SOG

Fig 1.1 Molecular structure of four types of SOGs.

temperatures (usually electron energies are ~10 to 100 times higher than that of gas molecules). After they gain sufficient energy by acceleration due to electric field, electrons undergo inelastic collisions and lose some of their energy. The energy transfer ratio is equal to 4Mm/(m+M), where M and m are the molecular mass and electron mass, respectively. Since the electron mass is relatively small compared to the gas molecules, the amount of energy transfer is very small (elastic collisions). Ultimately, higher energy excitation, dissociation, and ionization occurs by inelastic collisions.

The application of a voltage to a low pressure gas causes the gas molecules to be excited, dissociated, and ionized to a variety of electrons, ions, radicals, and molecules[32-34]. The charged species (ions and electrons) enable the plasma to transport current. Because the glow region is at a higher potential than the electrode, the potential difference accelerates positive ions onto the substrate positioned on the lower electrode, the energetic ions , along with reactive neutral spices which break bonds in the SOG. The organic groups react with oxygen atoms ,molecules or ions to remove carbon from the film and ultimately convert the material into a silicate glass.

Organic groups are very difficult to remove from siloxane films during low temperature annealing. In 1985, Butherus et al.[35] used oxygen plasmas to remove organic groups in SOG films, because the conversion from a polymeric

material to a silicate glass can be accomplished effectively by plasmas at low temperatures. This process is quite attractive in overcoming a limitation in the fabrication of devices if temperatures needed to form plasma deposited SiO_2 (>250°C) or to thermally convert SOG (>500^{0}C) cannot be tolerated. The likely mechanism for plasma conversion of SOG materials involves the formation of chemically reactive species in a plasma.

1.4 Objective

As device dimensions shrink into the submicron regime and packing densities continue to increase, the spin on glass (SOG) process may be the simplest method to planarize surfaces with severe topography.[36] The purpose of this research was to study films spin-cast from polysiloxane material (Dow Corning Z6032). The study began by establishing the relationships between spin speed, polymer concentration, and film thickness in the spin-cast films. Subsequently, film composition variations during heat treatment cycles and plasma treatments were studied. Finally, the optical and electronic properties of the films were determined in order to provide insight into the application of such materials in ULSI devices.

Chapter 2

Experimental Procedures and Analytical Techniques

2.1 Sample Preparation and Film Formation

The material chosen for this study was Dow Corning Z-6032 silane which contains vinylbenzyl amino and trimethoxysilyl groups, the chemicaal formula is

$(CH_3O)_3$-$SiCH_2CH_2CH_2NHCH_2CH_2NHCH_2$--  -$CH=CH_2$

This siloxane was dissolved in methanol.

The substrates used were (100) p type , 15-30 Ω-cm, 3 inch diameter silicon wafers. These wafers were precleaned by the following sequence of steps:

1. 5:1:1 H_2O:H_2O_2:NH_4OH at 75^0 C for 10 minutes. (SC1)
2. Deionized water rinse (5 times), each rinse time is ~1 minute.
3. 5:1:1 H_2O:H_2O_2:HCl at 65^0 C for 10 minutes.(SC2)
4. Deionized water rinse (5 times), each rinse time is ~1 minute.
5. 10:1 H_2O:HF etch (8 dips followed by a 15 second submersion).
6. Final deionized water rinse (7 times) , each rinse time is ~1 minute.
7. Dry spin for 5 minutes.

The SC1 step removes organic contamination and group IB and IIB impurities. The SC2 cleaning removes ionic impurities, while the 10:1 HF etch removes the silicon oxide formed during the cleaning process.

A Headway research spinner (EC101) was used to spin the 10 % silane

solution onto silicon wafers. The spin speed was 1600 rpm for 30 seconds to form a film with thickness ~ 200 nm. The coated wafers were prebaked at 100^{O}C in a convection oven for 1 hour to remove the solvent, and then placed in an oven to begin the curing process (heat treatment). Treatment temperatures ranged from 200 to 1000°C in 100 °C increments; the time for each treatment cycle was 30 minutes. The anneal cycles altered the film composition according to whether the film was exposed to air, nitrogen, oxygen , nitrogen with saturated water vapor, or oxygen with saturated water vapor.

2.2 Plasma- Converted SOG

A 10 % silane solution was spun onto a silicon wafer to yield a film of ~ 200 nm; the thickness variation between the center and edge of the wafer was~10 nm. Samples were plasma treated with a helical resonator generated oxygen plasma. One sample was used as control, while another sample was thermally treated. Two oxygen plasma treatments were used: one with the substrate electrically floating, and one under constant current anodization conditions. [37] The thermal treatment was performed at 30mtorr, 250 ^{0}C for 40 minutes, while the plasma treatments were performed at 30mtorr, 300W, 250^{0}C for 40 minutes; the constant current anodizations used a current density of 1.78 mamp/cm^{2}.

2.3 Film Analysis

Thickness and refractive index were measured with a Rudolph Research/Auto EL ellipsometer equipped with a 632.8 nm wavelength helium-neon laser; the incident angle was fixed at 70 ^{0}C. The measured del and psi values of the thin film were converted into corresponding thickness and refractive indices by a HP-85 microcomputer (Rudolf Program 10, 11, 13). The relative composition and film bonding structure were studied with a Mattson Instruments, Inc., Cygnus 25 Fourier Transform Infrared Spectrometer (FTIR). Chemical composition information was obtained by X-ray photoelectron spectroscopy (XPS) using non- monochromatic Mg Kα X-rays in a Kratos XSAM 800 surface analysis system.

2.4 Electrical Properties

Electrical properties of the films were determined by capacitance-voltage (CV) and current-voltage (I-V) analysis of metal-oxide-silicon (MOS) structures using a Hewlett-Packard 4280A C-V and 4145A I-V Plotters, respectively. CV characteristics of the MOS capacitors measure the effect of an applied bias on the bending of the semiconductor energy bands. A negative charge in the oxide shifts the CV plot to positive voltages while a positive oxide charge shifts the plot in the opposite direction. [38] By comparing theoretical and experimental CV plots, the fixed oxide charge density, and interface trap density can be determined from the flat band voltage shift and

metal-silicon work function differences[38,44]. The flat band voltage shift due to Q_f (fixed oxide charge) is given by $V_{fb,\ shift} = -Q_f/C_o$ where Q_f is in coulombs per square centimeter, and Co is the oxide capacitance in farads per square centimeter. Since Q_f is always a positive charge, the flat band shift is negative. Typical values of the V_{fb} shift from Q_f are -0.5V or less. Interface traps (D_{it}) are electronic states that reside at the oxide semiconductor interface as the result of dangling bond. Unlike Q_f, interface charges are charged or discharged (positive or negative, depending on whether the state is donor-like or acceptor-like) upon band bending. (ie, when the applied voltage is changed)

The dielectric constant was calculated from the measured capacitance, aluminum electrode area (~ 1.25×10^{-3} cm^2), and film thickness at the measurement frequency of 1 MHZ by using the formula $\varepsilon_r = Ct / \varepsilon_o A$, where ε_r is the relative dielectric constant, ε_o is the permittivity of vacuum with a value of 8.854×10^{12} F/M, C is the measured capacitance, t is the film thickness, and A is the capacitor area.

The fabrication sequence for MOS capacitors is:

1. Aluminum evaporation to ~ 50nm.
2. Apply OCG 820 positive photoresist, expose photoresist through mask for 3.1 second to define gate areas.
3. Immerse photoresist exposed wafer in KTI 809 to develop photoresist.

4. Immerse in the PAN (phosphoric:acetic:nitric:water:16:1:1:2) solution (45^0C for 1~5 mins) to etch Al.

5. Strip photoresist with ACT1 for 30 minutes, then rinse in DI water 5 times and spin dry for 10 minutes.

6. PMA (Post Metal Anneal) in forming gas(20% hydrogen and 80 % nitrogen) at 400^0C for 30 minutes.

2.5 Wet Etching

Wet etching rates were determined by the following sequences (Fig 2.1).

1. Place samples in oven at 120C for 30 minutes to drive off solvent.

2. Vapor prime with HMDS(hexamethyldisilazane) and xylene. The purpose of this is to promote adhesion between photoresist and siloxane surface.

3. Apply positive photoresist(OGT820) at a spin speed of 5000 r.p.m for 40 seconds.

4. Soft bake in oven at 92 ^{0}C for 30 minutes to evaporate solvent from photoresist.

5. Expose photoresist through mask for 3.1 seconds to define gate areas.

6. Immerse photoresist exposed wafers in KTI809 solution then spin dry for 10 minutes and hard bake at 120^0C for 30 minutes.

7. 1:500 (hydrofluoric acid: ammonium fluoride) solution was used to etch

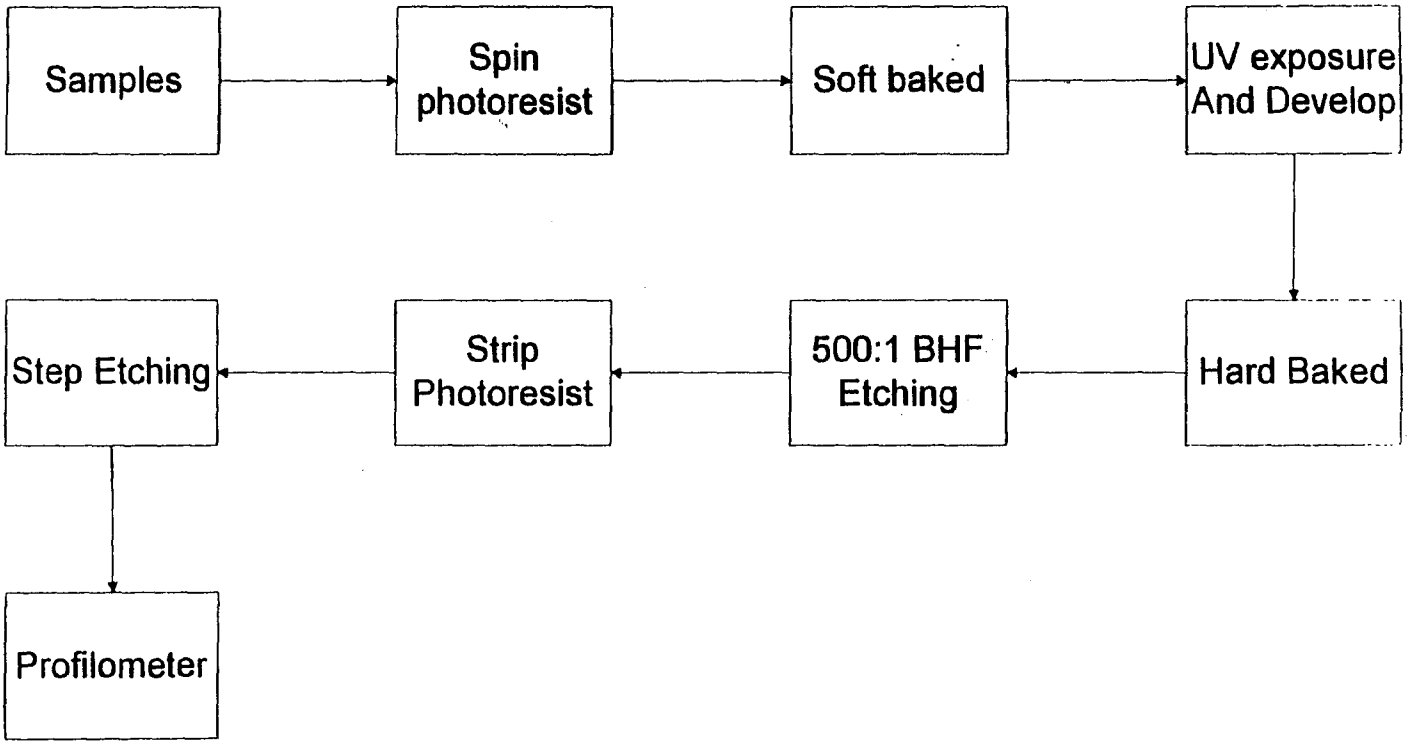

Fig 2.1 Flow Chart illustrating the BHF Etching Procedures and Measure Technique

samples for 2 minutes.

8. Strip photoresist with ACT1, then rinse in DI water 5 times and spin dry for 10 minutes.
9. Measure the etch depth by Tencor P-2 long scan profiler.

2.6 Dry Etching

The experimental procedures are as follows and are shown in Fig 2.2

1. Spin Shipley photoresist (1400-37) at 3500 rpm for 30 sec; the thickness of photoresist is ~ 3.0 um
2. UV exposure, 200mW/cm^2 for 7 sec.
3. Developed by Shipley developer(354), rinse in Deionized water and spin dry
4. Reactive ion etching (RIE), followed by SEM pictures.
5. Remove the remaining photoresist with acetone.
6. Measure the etching depth by profiler (Tencor Alpha- Step 500 surface profiler).

Fig 2.3 is a summary of the experimental procedure.

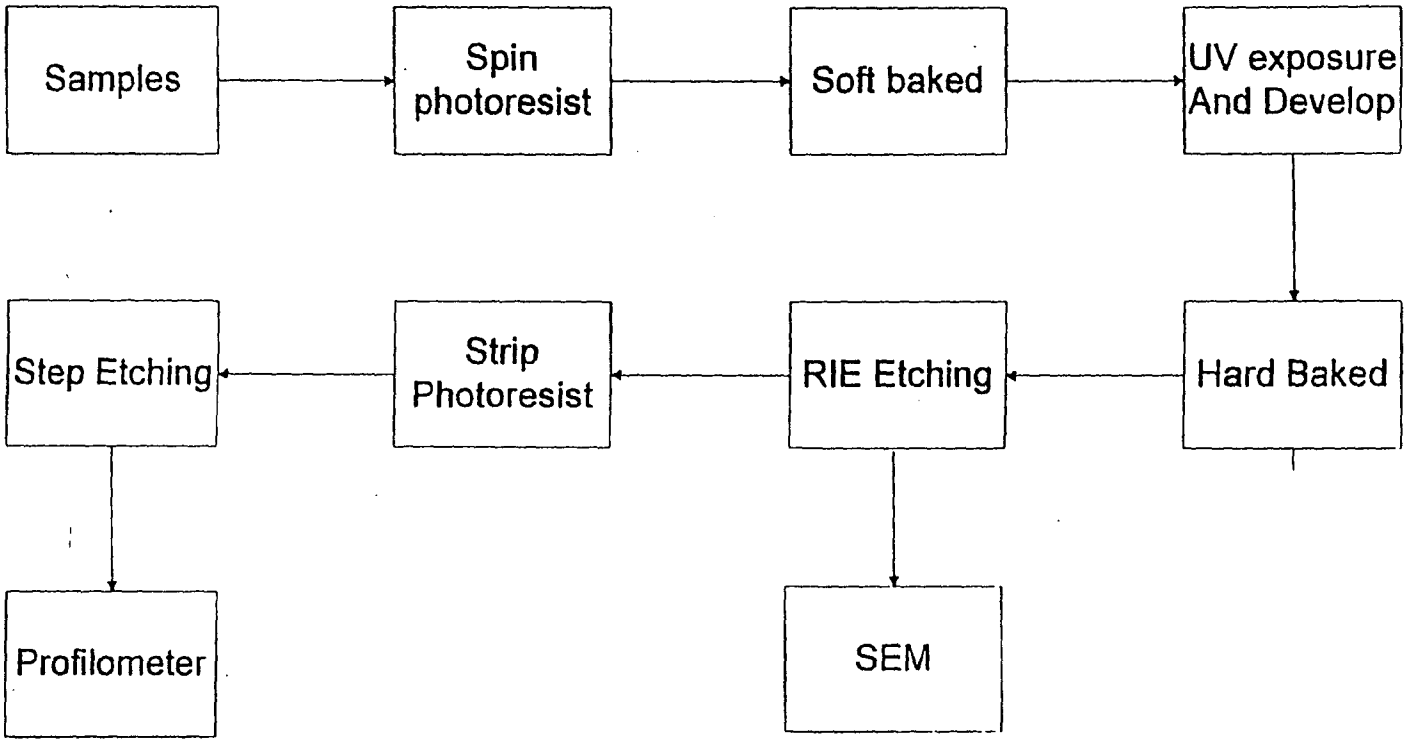

Fig 2.2. Flow Chart illustrating the RIE Etching Procedures and Measure Technique

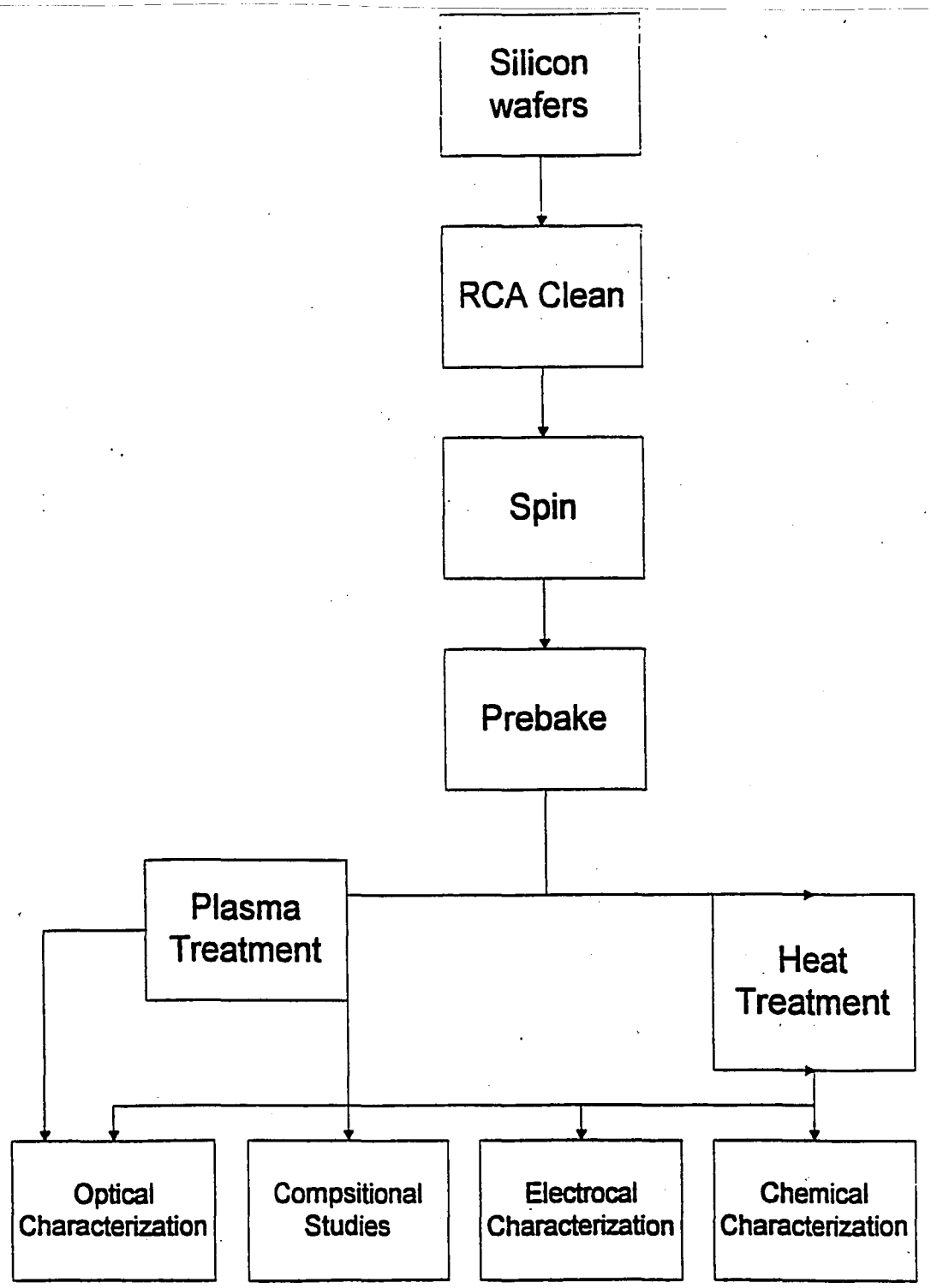

Fig 2.3 Experimental Procedure

Chapter 3

Result and Discussion

3.1 Spin Coating Study

Fig 3.1 shows the average film thickness as a function of spin speed for various solution concentrations. At a fixed solution concentration, the film thickness decreases as spin speed increases due to an increase of the angular velocity at higher spin speeds. The linear relationship of film thickness and spin speed is seen for solution ranging from 2%-10%. And this is consistent with results from other studies. [2,4,39] However, the 1% solution does not follow the linear relationship, probably due to the presence of pinholes in this very thin film which causes a fluctuation in thickness.[4]

In Fig 3.2, the spin speed and spin time are fixed at 1600 rpm and 30 seconds, respectively. The film thickness increases at higher concentrations due to the higher solution viscosity.[3, 4.39]

3.2 Film Formation Chemistry

The spin on glass (SOG) materials usually have various side chains. These side chains may be inert organic groups such as $-CH_3$, $-C_2H_5$, $-C_6H_5$, or reactive groups such as -OH, $-CH_3$,- OC_2H_5. These reactive side chains can react with other molecules to form highly polymerized materials with combined organic/inorganic characteristics.

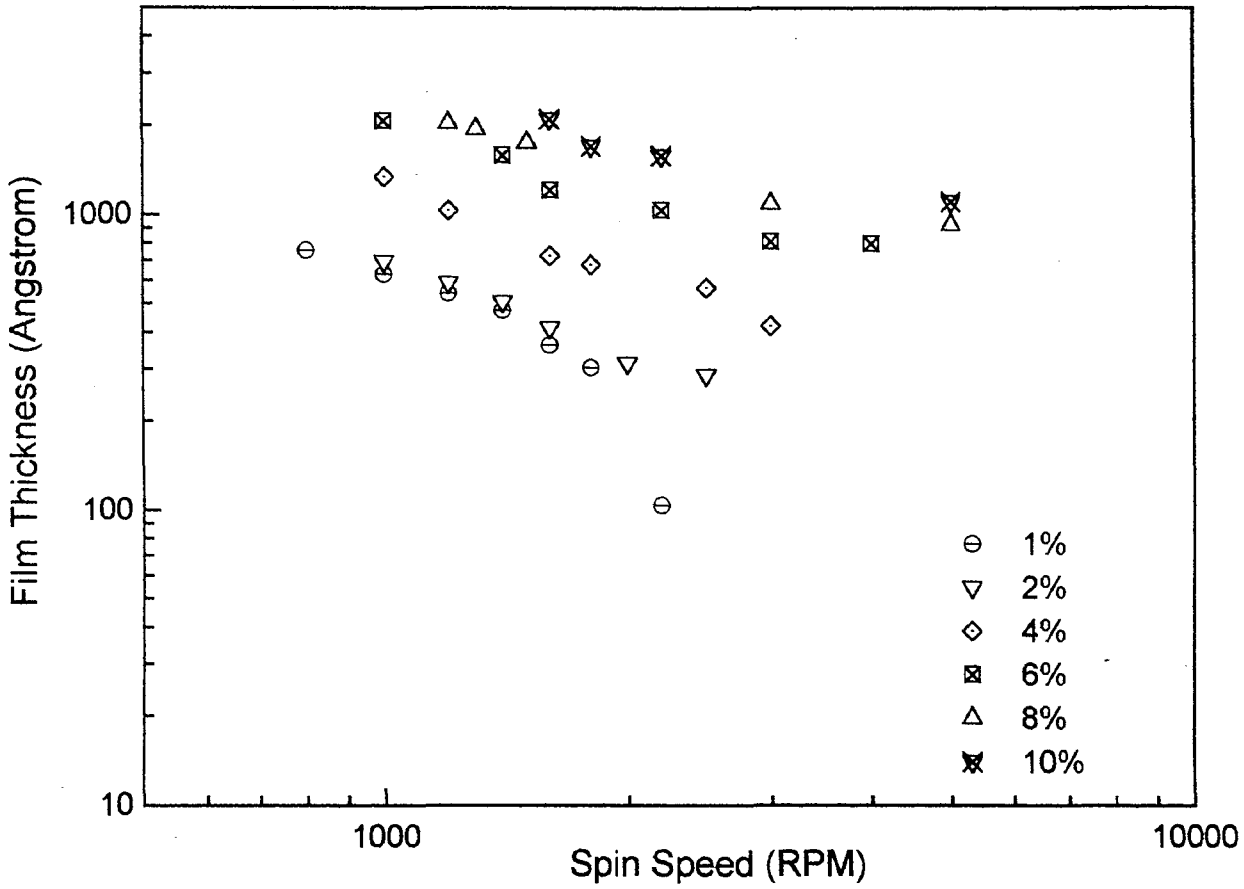

Fig.3.1 Measured film thickness as a function of spin speed (rpm) and solution concentration

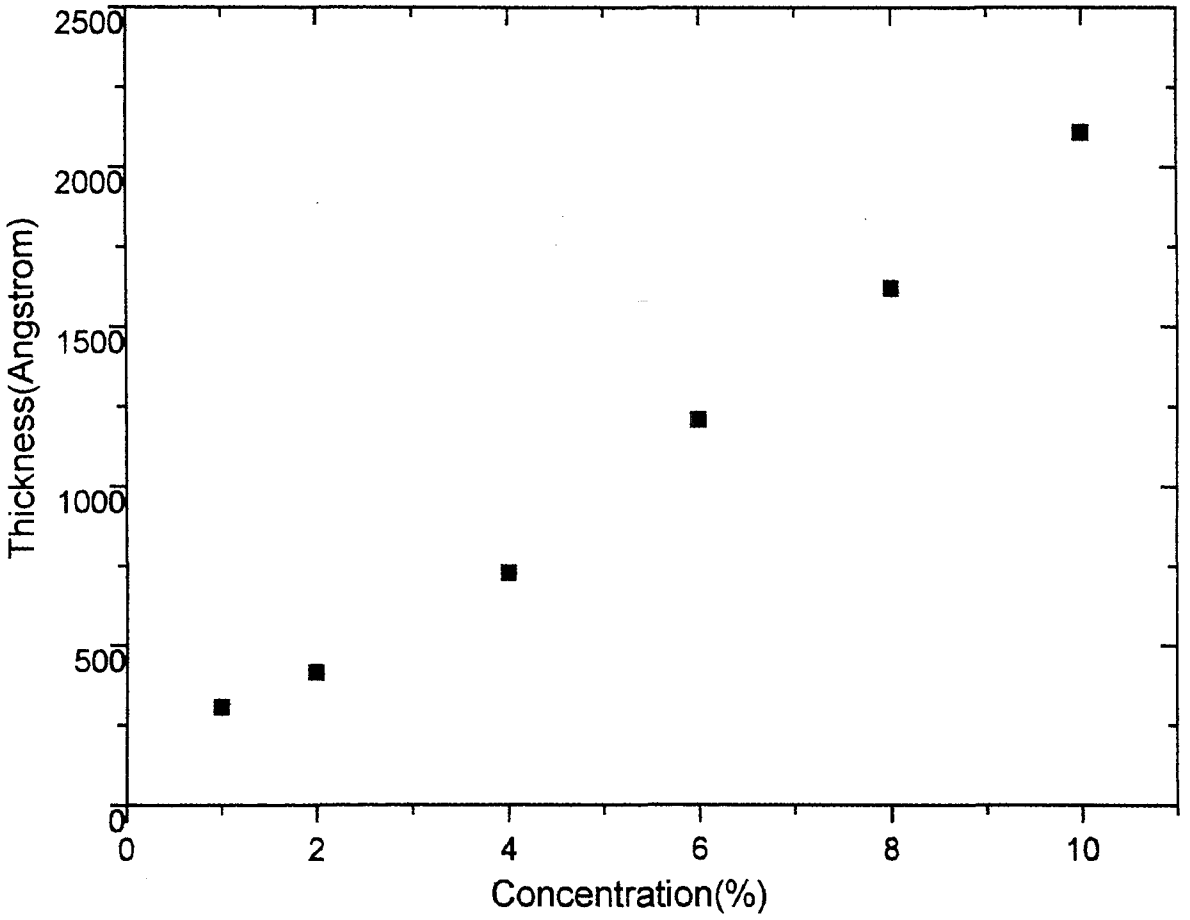

Fig.3.2 Measured film thickness as a function of the initial solution concentration (%) at 1600 rpm and 30 second.

Step 1: Hydrolysis

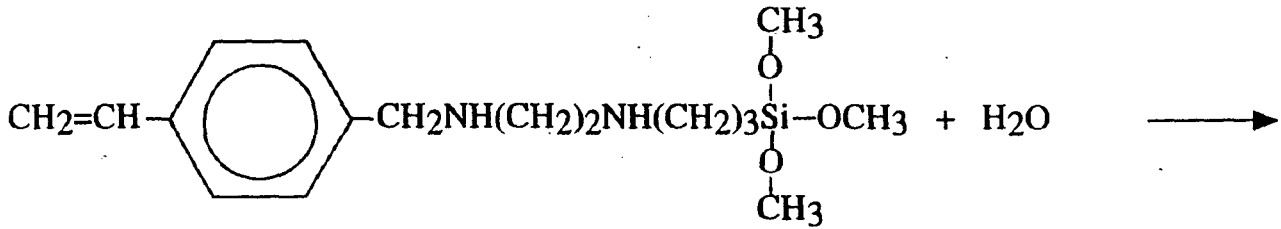

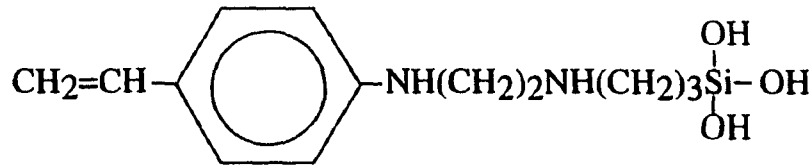

Step 2: Condensation

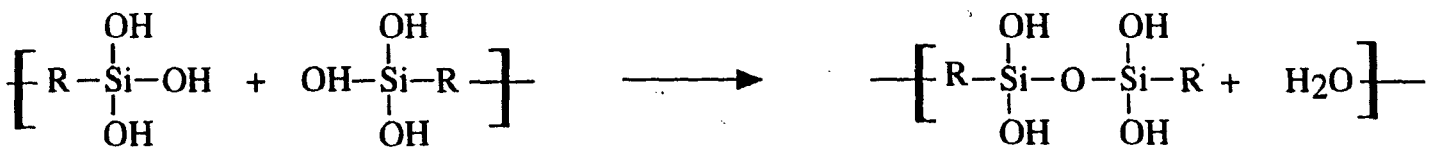

Fig.3.3 Possible film formation mechanism.

The film formation chemistry of various SOG films are shown in other studies.[26,35] The film formation is dominated by hydrolysis and condensation reactions. The likely film formation mechanism is shown in Fig.3.3. In the molecular structure of the precursor, there are 3 reactive methoxy groups. These three -OCH_3 groups can react with water molecules to form highly polymerized material with combined organic/inorganic characteristics. The -OCH_3 first reacts with water and forms Si-OH; then condensation reactions occur as the material is heated and cured. In this stage, crosslinking occurs by water release at relatively low temperatures (<300^0C) to form a siloxane polymer with a backbone of alternating silicon and oxygen atoms.

3.3 Film Composition Study

A. Fourier Transform Infrared Spectroscopy (FTIR)

Table 3.1 summarizes the infrared vibrational assignments.[40] An FTIR spectrum of the as-spun polysiloxane film is shown for wavenumbers between 4000-500 cm^{-1} in Fig 3.4. This spectrum indicates that the principal bonding structures present in the film are Si-O stretching (1000-1150 cm^{-1}), C-H stretching (2936-2812cm^{-1}), Si-C stretching (1200cm^{-1}), O-H stretching (3200-3700cm^{-1}), and N-H stretching (3350m^{-1}). The O-H stretching feature can account for the Si-OH bonding during the hydrolysis reaction. The N-H stretching feature represents the N-H bond in the precursor. The C-H

Table 3.1 Infrared Absorption peak assignment.

Wavenumber (1/cm)	Assignment
3200-3700	O-H streching
3350	N-H stretching
2938	CH_3 antisymmetric stretching
2812	CH_2 antisymmetric stretching
1200	Si-C stretching
1100-1150	Si-O-Si symmetric stretching
1090-1070	Si-O asymmetric stretching
940	Si-OH stretching

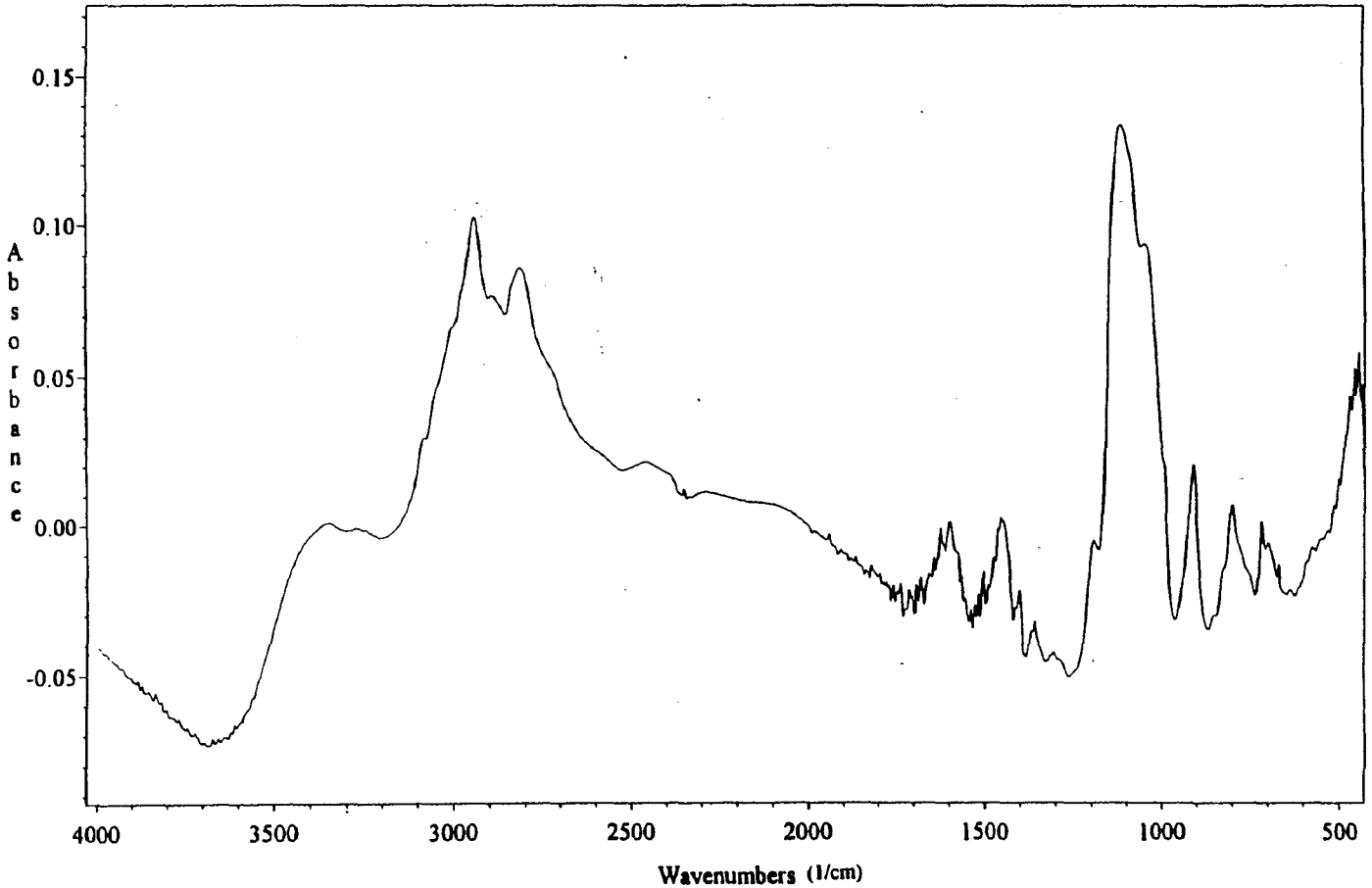

Fig. 3.4 FTIR spectra of as-spun film at room temperature, film thickness is ~200nm.

stretching vibration may correspond to the molecules of $Si(OCH_3)$or CH_3OH. The $Si(OCH_3)$ and CH_3OH peaks result from the evaporation of the organic solvent when the solution completes the sol-gel step and hardens into the porous glass films.

In the Si-O stretching region, the FTIR spectrum shows the silicon-oxygen stretch as a double peaks. Previous studies have defined this as a "Fermi resonance effect" which accounts for substances displaying two peaks of the same nature in the IR spectrum.[41] Here, the double peaks are part of the same molecule, but have different bonding environments. The asymmetric Si-O stretch (1090-1070 cm^{-1}) and symmetric Si-O-Si stretching (1100-1150 cm^{-1}) account for these two peaks.

Additionally, the Si-C stretching feature also exists for the SOG film. Nakano [42] et al. have proposed 1200 cm^{-1} as the Si-C vibration. Thus, we assign the peak at 1200 cm^{-1} as the Si-C stretching vibration.

The FTIR spectra observed at different temperatures (200-1000^{0}C) after various anneals are shown in Fig 3.5-3.9. Nitrogen annealed samples (Fig.3.6) show a decrease of the Si-O-Si symmetric stretching peak (1131cm^{-1}) and Si-C peak (1200 cm^{-1}) from 200 to 400 ^{0}C. Above 400^{0}C, the double peak is dominated by the Si-O asymmetric stretching. This suggests that Si-O-Si reacts with H_2O to form Si-OH, thereby, changing the bonding

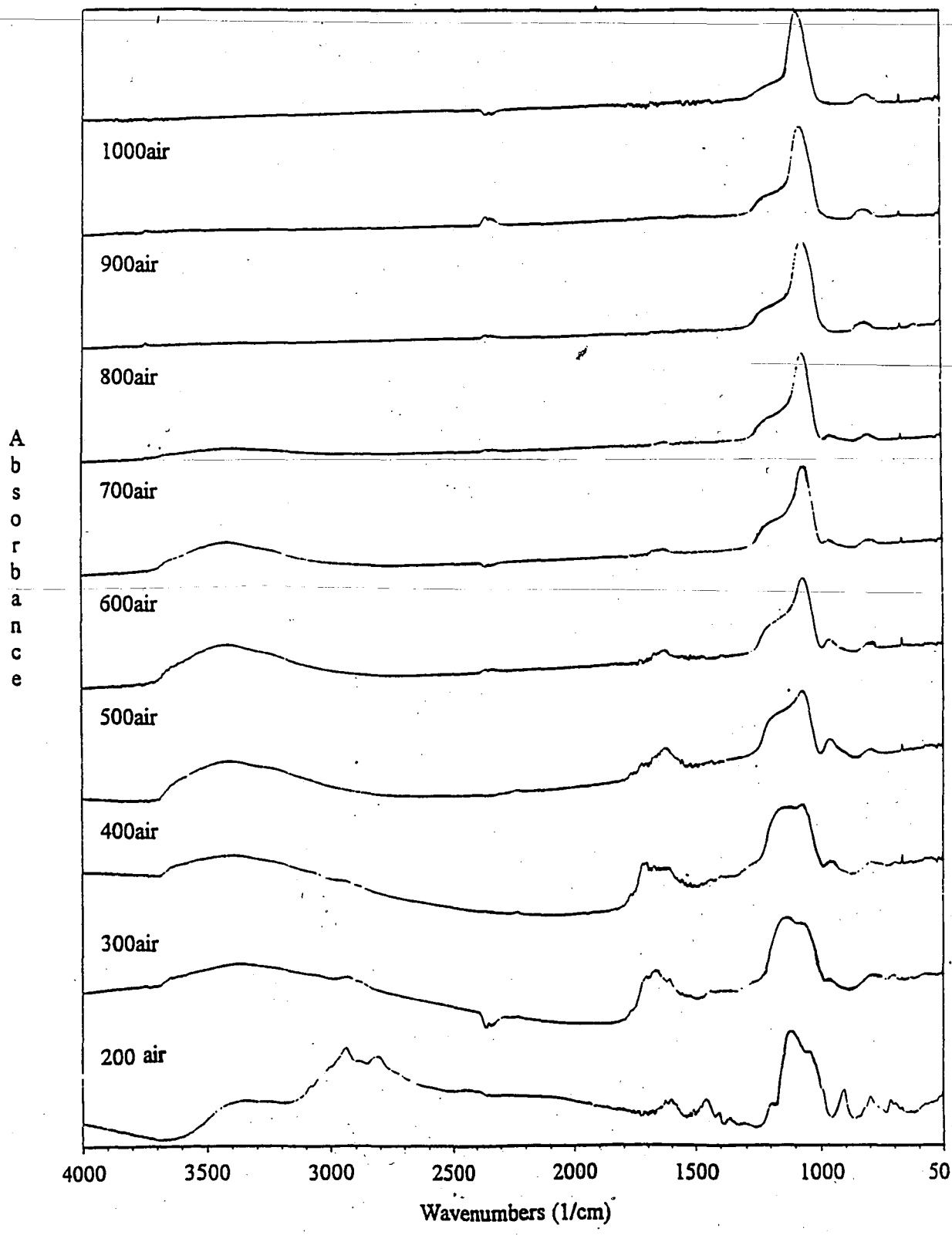

Fig. 3.5 FTIR spectra of as-spun films between 200-1000^{0}C in air ambient.

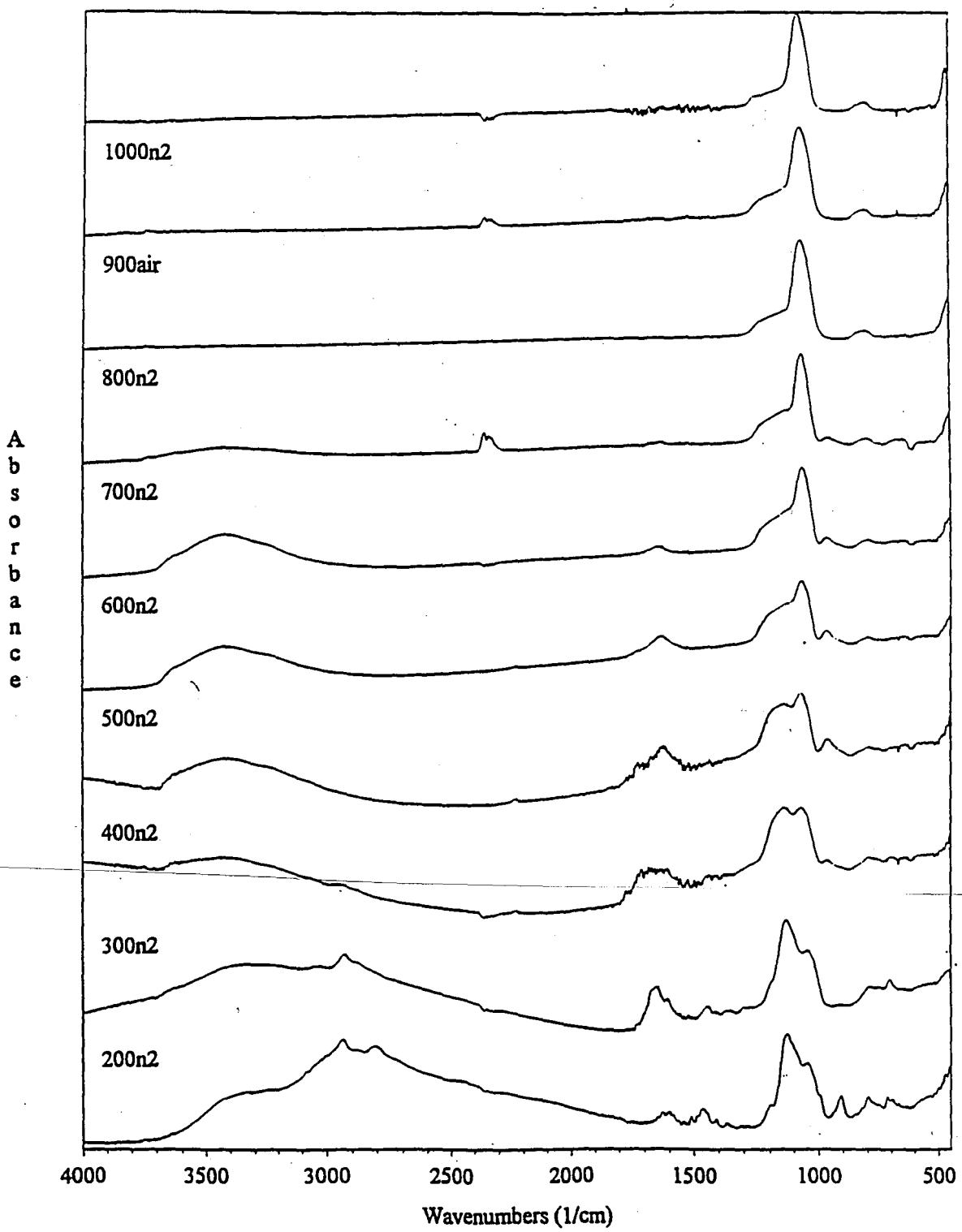

Fig. 3.6 FTIR spectra of as-spun films between 200-1000^{0}C in nitrogen ambient.

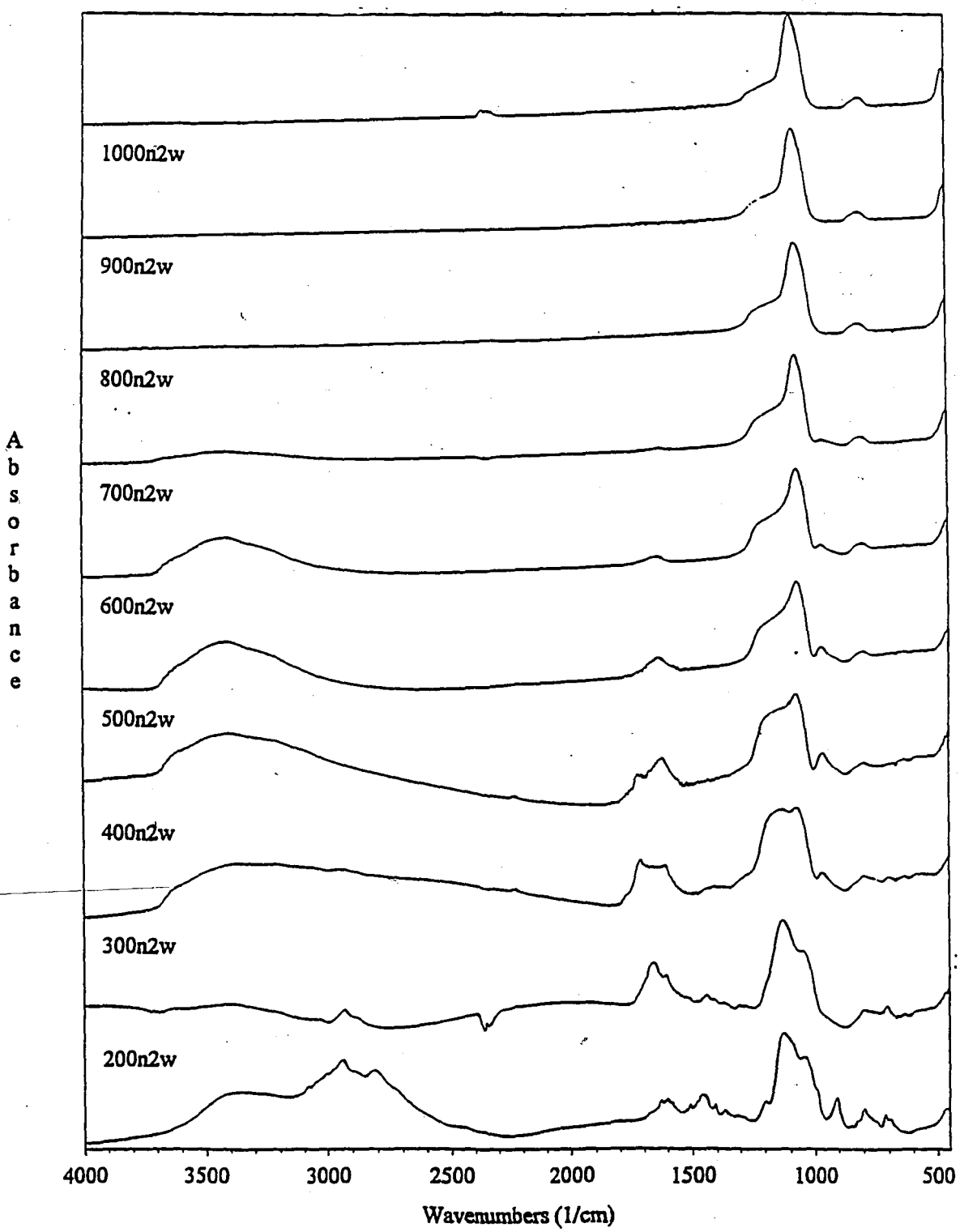

Fig. 3.7 FTIR spectra of as-spun films between 200-1000^{0}C in nitrogen with saturated water vapor.

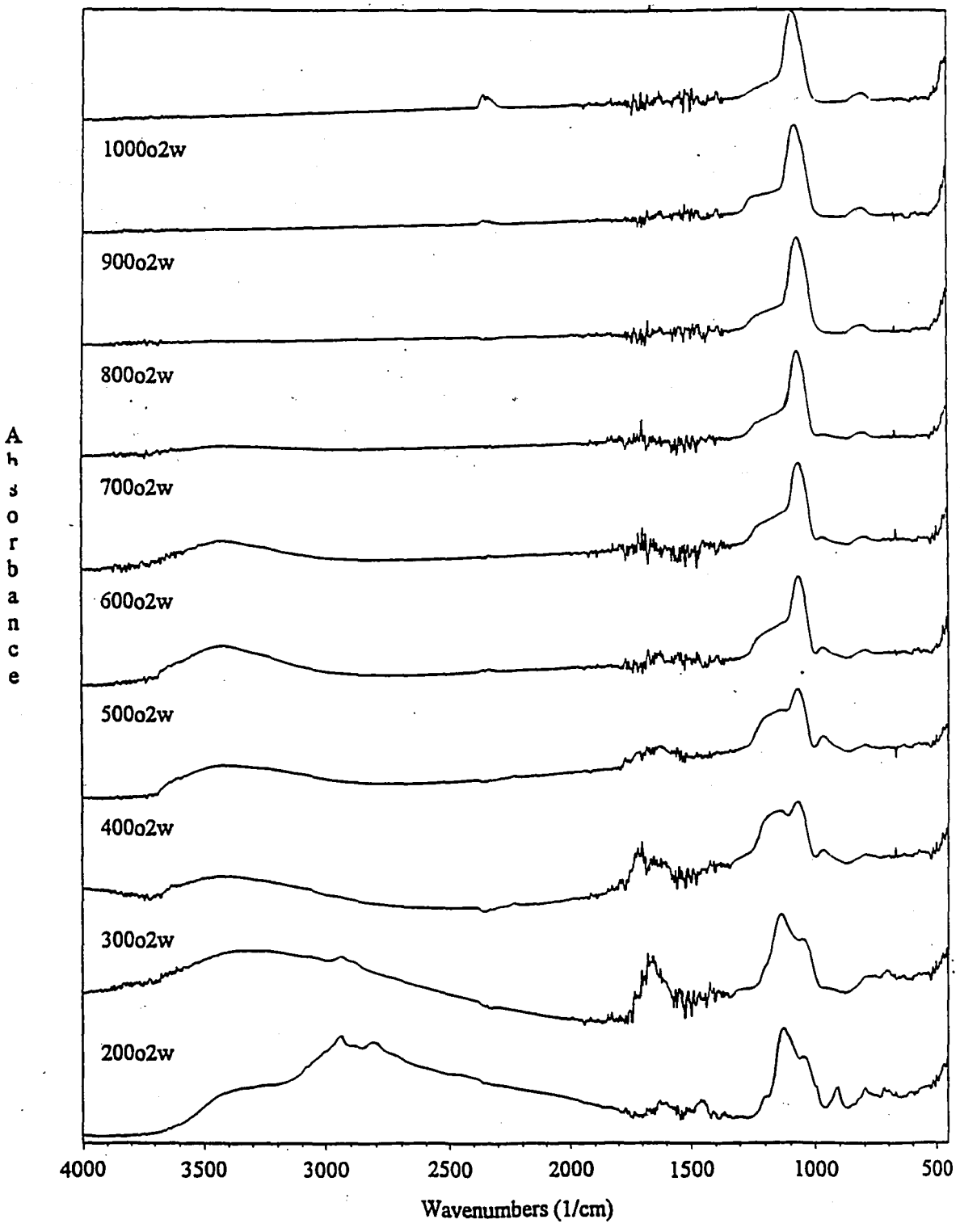

Fig. 3.8 FTIR spectra of as-spun films between 200-1000^{0}C in oxygen with saturated water vapor.

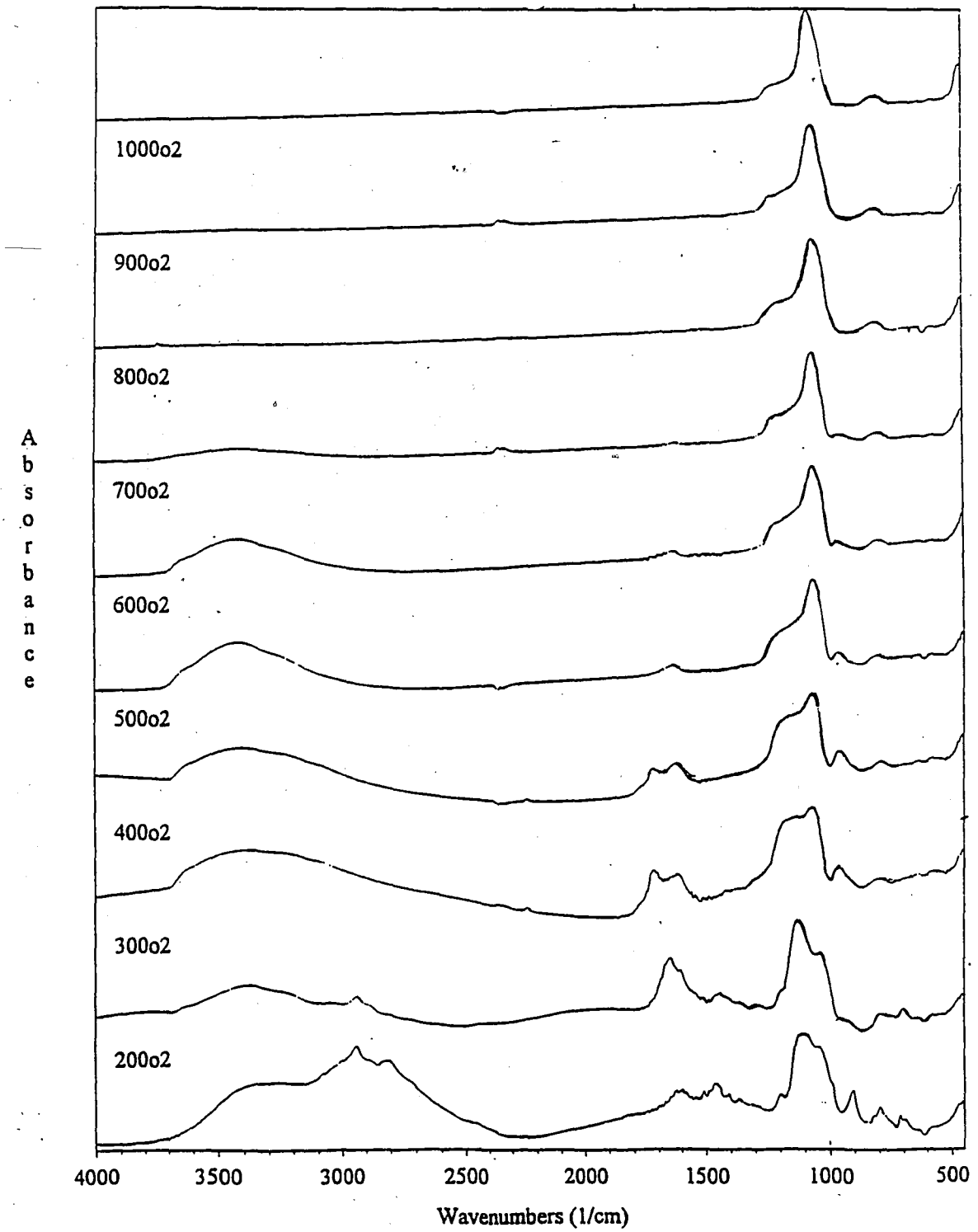

Fig. 3.9 FTIR spectra of as-spun films between 200-1000^{0}C in oxygen ambient.

environment of the Si-O peak. As the temperature increases, the Si-O asymmetric peak becomes even sharper until it finally becomes more like that from thermal oxides with a peak absorbance at ~1085cm^{-1} at temperatures above 800^{0}C . These results suggest that the Si-O peak is sensitive to the annealing temperature. Compared with other ambients, the Si-O asymmetric stretching peak domination showed up at earlier temperatures between 200 to 300^{0}C except in the nitrogen annealing conditions. This observation suggests that the oxygen-containing (dry oxygen or moisture-containing) assist in oxidizing the polysiloxane films.

Compared with other studies [43], no observation about the two peaks transition phenomena in TEOS/alcohol/H_2O spin on glass film. the film annealed at 400^{0}C in oxygen, the peak has located in the thermal oxide region. In the other silicate glass film study [53], the more like thermal oxide with wavenumber 1080cm^{-1} appears at 1200^{0}C. This suggests that TESO-based SOG film is easier to convert to more like thermal oxide than silicate glass and trimethoxy-based films at lower anneal temperature.

Ambients that contain oxygen play a more aggressive role than nitrogen in removing organic components. In addition, the increase of annealing temperatures cause elimination of the C-H (2936-2812cm^{-1}) features for all annealing ambients. This indicates that the organic components, and residual

solvent, decompose and outgas from the film as annealing temperatures are elevated in all ambients. When the solution is spun onto the wafer, the CH_3 ($2939cm^{-1}$) and CH_2 ($2812cm^{-1}$) features are distinct, as shown in Fig 3.4. As the temperature exceeds 400^0C, these peaks disappear because the residual methanol solvent evaporates from the film and organic groups decompose. Fig 3.10 shows the position changes of Si-O IR absorption as a function of annealing temperature. In general , between 300^0C and 600^0C, the Si-O peak shifts from higher wavenumber to lower wavenumber because of initial solvent evaporation or cross- linking of the siloxane network. Apparently, the position of this peak (Si-O) must be related to the complicated compositional changes that occur during the curing process. The presence of water, solvent, organic groups, and silanol have each contributed to the position and strength of Si-O peak. At $600\ ^0C$, Si-O peak reaches a glass transition point for all annealing ambients. This suggests that most organic groups are removed from the film, and as glass densification occurs, the siloxane is converted into a silicate structure. After 800^0C annealing, the wave number continues to increase for all ambients and becomes more like that of oxides with a wavenumber of $\sim 1085\ cm^{-1}$. This phenomenon is consistent with other studies which show that upon high temperature annealing, the properties of SOG films become more like thermal oxides. Our data reconfirm the findings in other

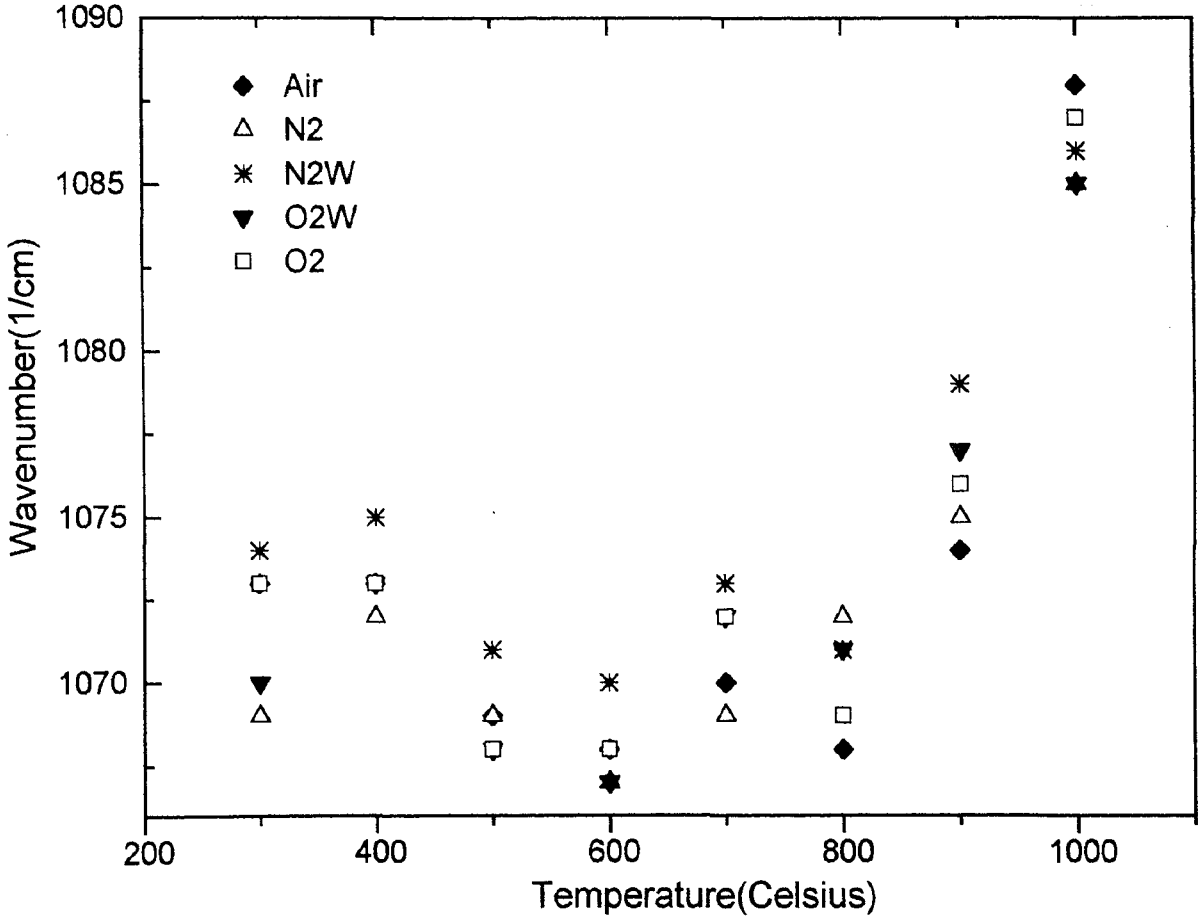

Fig.3.10 Position of Si-O IR absorption as a function of annealing temperatures.

studies [41, 45, 46], the Si-O peak position approaches to 1080cm^{-1} above 800^{0}C annealed.

I believe that the ratio of the area under the Si-O asymmetric stretching and Si-O-Si symmetric stretching is an indicator of the relatively film densification. The ratio of the two Si-O peaks in 400^{0}C nitrogen annealed samples (Fig 3.6) approaches 1 whereas the ratio is greater than 1 for other ambients at the same temperature. Thus, nitrogen is not as effective as the other oxygen-containing ambients in changing the bonding environment of Si-O features. Between 400^{0}C and 600^{0}C, the area under the asymmetric Si-O peak becomes larger than the area under the symmetric Si-O-Si peak. This suggests that compositional changes and densification occur in this temperature region. This has been investigated by other investigators.[47] The difference between my observation and others is that the ratio of the integrated area (Si-O asymmetric/Si-O-Si) in my result shows increase from 200-400^{0}C in nitrogen and oxygen annealed. Other investigator show that the ratio is almost equal in oxygen and nitrogen annealed at 200-400^{0}C. [47]

The interaction of H_2O with SiO_2 has been investigated by several studies [48-52], they propose a similar model for adsorption and desorption sites in silicate and CVD oxides, respectively. Theil et al.[50,51] have investigated the interaction for remote plasma enhanced CVD (RPECVD) and propose several

reaction pathways and sources of Si-OH groups. Tompkins et al. [43, 52] has proposed three different adsorption sites for OH/H_2O in porous SiO_2: an isolated silanol group, a H_2O molecule which is hydrogen bonded to a silanol group (H bonded water), and two silanol groups which are hydrogen bonded to each other (H-bonded silanol). A schematic of various OH species in SOG films proposed by Tompkins is shown in Fig.3.11. It should be noted that hydrogen bonded silanols do not need to be next to each other, but the distance must to be close enough for reaction.

The reaction of Si-O-Si and water (H_2O) to give two Si-OH groups is considered reversible. Moisture interaction with the films alters the stress state and results in the relaxation of the Si-O-Si bond. Nakamura et al.[53] has reported that when SOG films are annealed below 600^0C, strained Si-O-Si was formed and relaxation occurred when Si-O-Si interacted with moisture to form Si-OH. This is consistent with the fact that the Si-O-Si symmetric stretching peak changes into an asymmetric stretch as the temperature wase raised from 200-400^0C in Fig.3.5-3.9.

The Si-OH vibrational frequencies are strongly influenced by hydrogen- bonding interactions. When hydrogen- bonding increases in the organic materials, the frequcncy of the O-H stretching vibration shifts to a lower wavenumber. Theil et al.[50,51] have noted that in REPECVD oxides, when the hydrogen bonding (O.....OH) distance decreases, the hydrogen

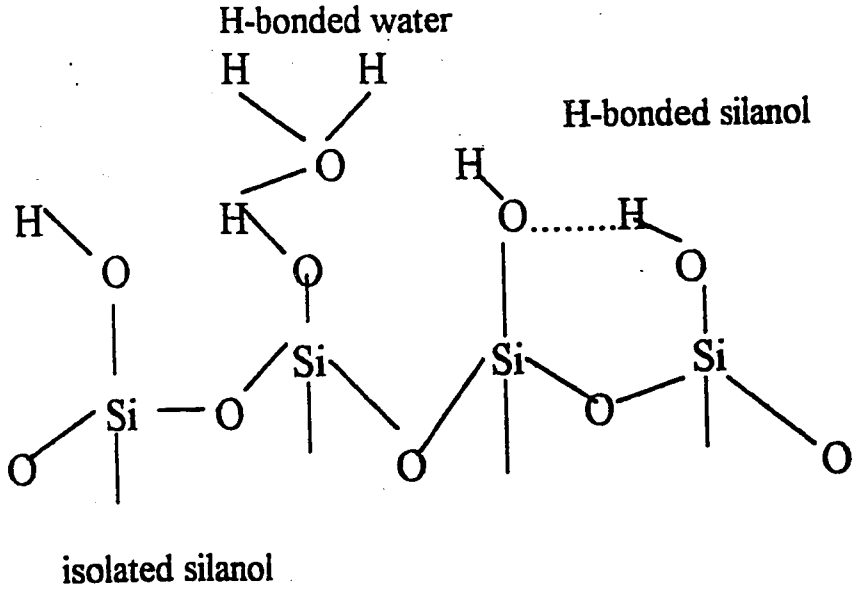

Fig. 3.11 Schematic drawing of various OH species in SOG.

bonding strength increases which results in a wavenumber shift from between 50-200 cm^{-1} in the 3200-3700cm^{-1} region.

Following Wood [48,49] and Theil [50,51], the peak at 3450 cm^{-1} which has a 3700cm^{-1} shoulder is identified as isolated silanol group and the peak at 3400 cm^{-1} as the hydrogen bonded silanol in Figs 3.5-3.9. The original peak center at ~3450cm^{-1} shifts to ~3500cm^{-1} as the temperature rises from 200-600^{0}C. This can be explained by the fact that the Si-OH local bonding environment has changed, from hydrogen bonded silanol to isolated silanol (or near isolated silanol). In our results, the feature is still centers at 3500 cm^{-1} (isolated silanol) at 700^{0}C which suggests that some isolated silanol is left in the film. At 800^{0}C, there is no clear observation about isolated silanol groups at 3500cm^{-1}. There are differences between my result and Wood's observation. Wood shows that in order to remove hydrogen-bonded water only at relatively high temperature (>800^{0}C) in silicate glass films[49]. In our observation, the hydrogen-bonded water can be removed at 400^{0}C and isolated silanol can be removed effectively at 800^{0}C in trimethoxy-based siloxane films.

The reason that isolated silanol can be removed above 800^{0}C can be explained by the relationship of viscosity and relaxation. As the anneal temperature increases , the glass viscosity becomes smaller and smaller which results in a more rapid relaxation rate of Si-O-Si.. This relaxation and

densification is detrimental to the driving force for Si-O-Si to reabsorb water. Thus, the extent of isolated silanol bonding decreases. This similar phenomenon was also observed by other studies in silicate glass films [53] and CVD oxide film [54]

Theil et al [50,51] have demonstrated that the absorption at 940 cm^{-1} is associated with the presence of the silanol functionality in the remote PECVD oxide. Following him, the feature at 3450cm^{-1} is correlated with the 940 cm^{-1} feature at 300^{0}C in Fig 3.5-3.9. The 3450cm^{-1} band arises from (Si-OH) stretching coupled with internal bending displacement of the hydroxyl group in strongly hydrogen bonded silanol. Between 300 and 600^{0}C, the intensity of this peak increases with the replacement of isolated silanol by the hydrogen bonded (or hydrogen bonded water silanol). At 800^{0}C, the 940cm^{-1} peak is not clearly observed probably due to the effective removal of isolated silanol. This is consistent with the disappearance of the 3500cm^{-1} peak at 800^{0}C.

B. X-Ray Photoelectron Spectroscopy (XPS) Studies

Elemental composition and chemical bonding structures in the SOG film were analyzed via XPS. Table 3.2 lists atomic % of Si2S, O1S, N1S, and C1S, and the ratio of O/Si, and C/Si for as-cast and annealed films . Fig 3.12 is a plot of film composition at room temperature, 400^{0}C, 600^{0}C, 800^{0}C, and 1000^{0}C for the nitrogen annealed samples. Both carbon and

	25^{0}C	400^{0}C	600^{0}C	800^{0}C	1000^{0}C
Si2P	4%	17%	30%	35%	36%
O1S	10%	22%	39%	42%	50%
N1S	7%	5%	4%	1%	0%
C1S	79%	56%	27%	22%	13%
O/Si	2.3	1.3	1.3	1.2	1.4
C/Si	17.9	3.3	0.9	0.6	0.4

Table 3.2 Atomic % for Si2S, O1S, N1S, C1S, O/Si, and C/Si in nitrogen annealed samples.

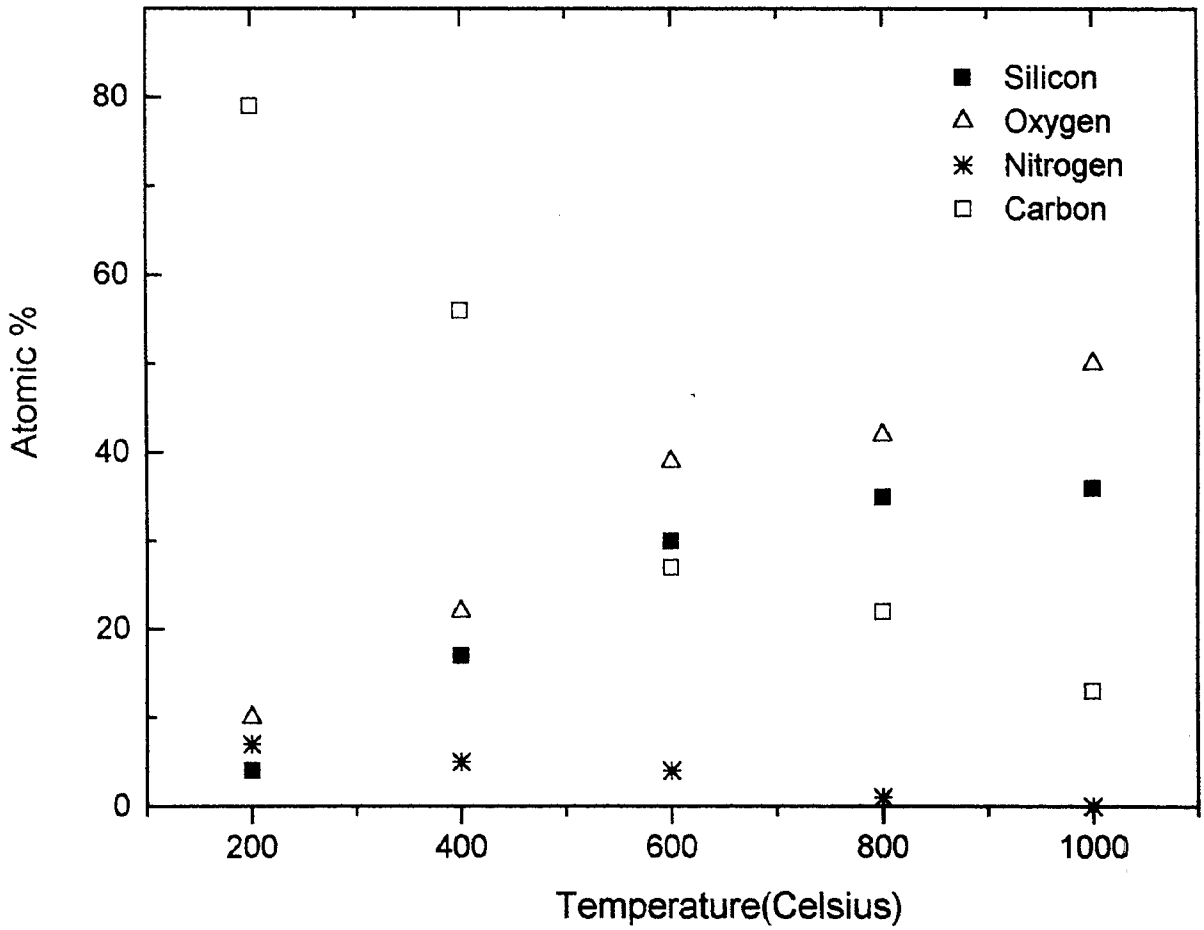

Fig 3.12 Atomic % as a function of annealing temperature

nitrogen percentages decrease as the temperature is raised, while the percentage of silicon and oxygen increases with increasing temperature. As listed in Table 3.2, the C/Si ratio decreases from 17.9 to 3.3 for the as spun and 400^{0}C nitrogen annealed samples, respectively. As the temperature approaches 400^{0}C, the nitrogen ambient begins to pyrolyze the film and reduce the overall carbon content. Between 400^{0}C and 600^{0}C, the carbon percentage continues to drop because most organic groups are being removed from the SOG films. This is in agreement with the FTIR results as shown in Fig 3.6; the drop in intensity of the C-H (2936-2812cm^{-1}) stretching vibration indicates that the organic group elimination by the 600^{0}C anneal. After a 600^{0}C anneal in nitrogen , the C/Si ratio continues to drop to 0.4. The O/Si ratio of 2.3 for as spun drops to 1.3 when the temperature reaches 400^{0}C. The likely reason may be related to Tompkin's et al [52] investigation that at 400^{0}C, SOG has significant water desorption which can account for the large O/Si large ratio drop. From 400^{0}C to 1000^{0}C, the ratio of O/Si stays at approximately 1.3. The ratio of O/Si at 1000^{0}C is 1.4 may be related to the oxidation occurs in the interface.

3.4 Film Shrinkage:

The SOG film thickness was measured after each 30 minutes of annealing. Table 3.3 displays the film shrinkage as a function of annealing

conditions. As the annealing temperature increases from 200-300^{0}C, solvent evaporates, organic groups decompose fragments and outgas from the films, thereby causing film shrinkage. This is consistent with the IR spectra in Fig.3.4-3.9; between 200 and 300^{0}C, the intensity of C-H (2936-2812cm^{-1}) bonds decreases. In addition, between 200 and 400^{0}C, films treated in nitrogen gas show the lowest thickness decrease (~74.7 nm) while the oxygen with saturated water vapor treatment shows the largest thickness decrease (~144.5 nm). This suggests that oxygen with water in the ambient is more effective in oxidizing organic groups than is a pure dry nitrogen anneal at lower temperature. This is consistent with Pliskin's [46] proposal that steam or the presence of moisture is more effective than dry ambients in densifing pyrolytic SiO_2 films and CVD oxide films. When the temperature exceeds 500^{0}C, the film thickness increases as a result of glass densification for all annealing ambients. Above 500^{0}C, there is less film shrinkage during the anneal step, because most of the organic groups have already outgassed from the film. When the temperature exceeds 500^{0}C, films treated in nitrogen exhibit continual film shrinkage, while films treated in other ambients exhibit little or no film shrinkage from 600- 800^{0}C. Above 800^{0}C, all the films, except for nitrogen annealed displayed a thickness increase relative to the preceeding anneals which suggests that thermal oxidation influences the total

Unit of thickness is(Angstrom)

	Air	N_2	N_2/H_2O	O_2/H_2O	O_2
25(^{0}C)	1990	1947	1965	2027	1969
200(^{0}C)	1380	1318	1204	1085	1192
300(^{0}C)	756	875	718	582	576
400(^{0}C)	518	571	563	503	476
500(^{0}C)	440	482	445	403	396
600(^{0}C)	389	419	392	419	371
800(^{0}C)	446	403	474	504	483
1000(^{0}C)	1216	321	854	1258	1000

Table 3.3 Film thickness variation as a function of anneal temperatures and ambients.

film thickness. The assumption that oxygen species diffuse through the films to the SOG -silicon interface is supported by the fact that the sample treated in nitrogen shows continual film shrinkage. At 1000^{0}C, ambients with increasing amounts of oxygen and moisture show greater thickness increases compared to the 800^{0}C.

3.5 Index of Refraction

The change in refractive index of the SOG film with annealing temperature (300-1000^{0}C) is shown in Fig 3. 13. Refractive index ranges from 1.40-1.66, and in general, are consistent with the composition changes in the SOG films. The original refractive index after spinning is ~1.56 because of the high organic film content. For the most part, the refractive index decreases as the annealing temperature increases. At 600^{0}C, the refractive indices for all anneal ambients drop to ~1.44; 600^{0}C can be regarded as a glass transition point. This suggests that the SOG is undergoing densification which causes a stoichiometric rearrangement in the Si-O network at this temperature. After 600^{0}C, as the result of the refractive indices increase and ultimately become more like thermal oxides with refractive index 1.46 [46] due to glass densification and the continual removal of organic groups. Indeed, refractive index can be used as one indicates of film's properties. For instance, between 200-600^{0}C , porosity exists in all films, but after 600^{0}C anneals, the refractive indices

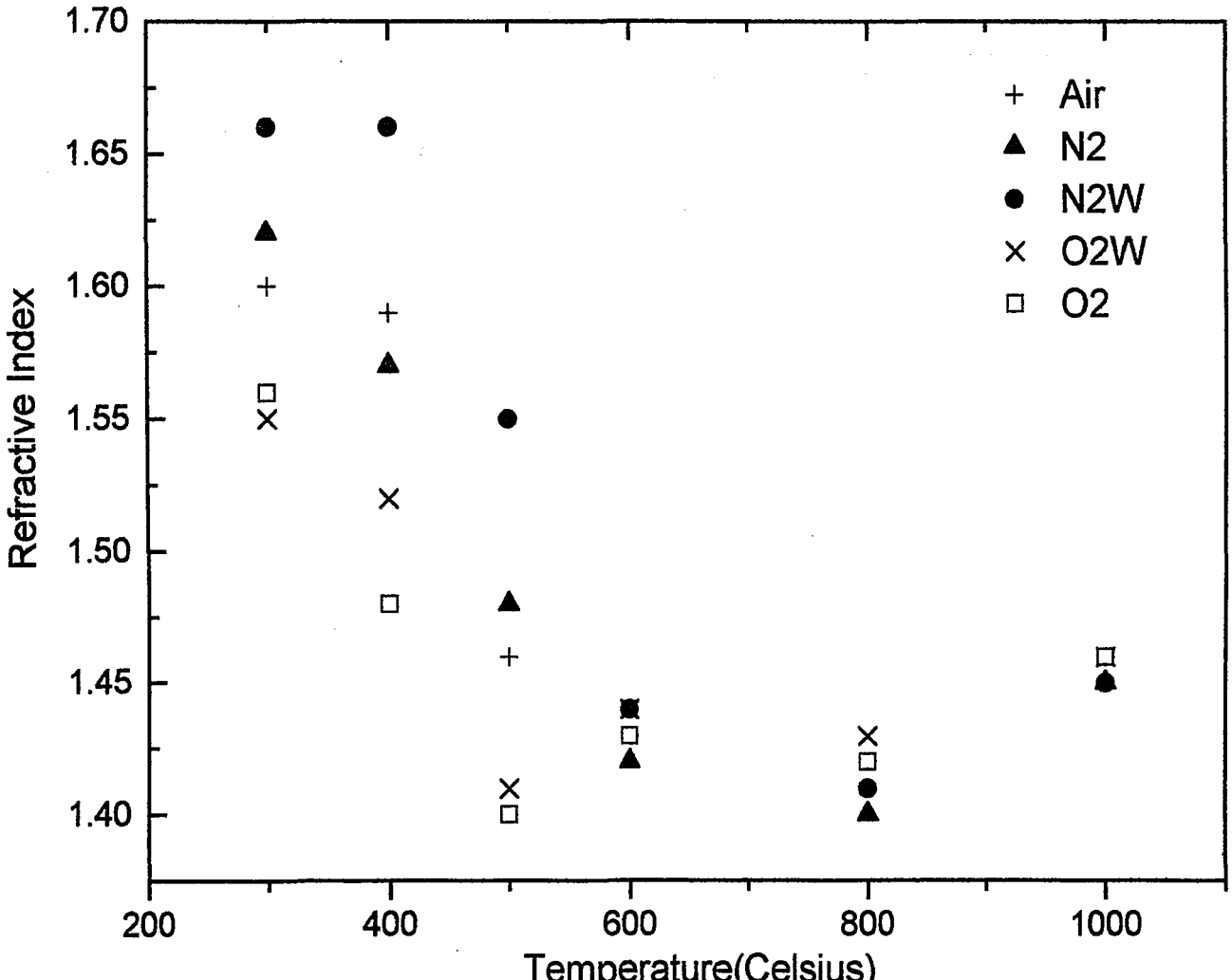

Fig 3.13 Refractive index as a function of anneal temperature

increase as the films become more dense (less porous) for all annealing ambients.

3.6 Oxygen Plasma-Converted SOG Material

The as-spun films were treated under several plasma conditions. Fig 3.14 shows an FTIR spectrum after oxygen treatment at 30mTorr, 250^{0}C for 40 minutes (no plasma). Fig 3.15 shows an FTIR spectrum of film after exposure to an oxygen plasma at 30mTorr, 300W, 250^{0}C, for 40 minutes with the substrate holder (substrate/film) at floating potential. Fig 3.16 is the FTIR spectrum after oxygen plasma anodization at 30 mTorr, 300W, current density of 1.78 mamp/cm^2 and 250^{0}C for 40 mins. The main difference between plasma oxidation and thermal oxidation is that the silicon and the as-spun polysiloxane films are exposed to reactive ions, electrons and atomic oxygen species during the plasma oxidation process. [55-59] Also, the main difference between plasma floating and constant current anodization is that in anodization, a positive bias is applied to the wafer, and the voltage is varied with time to maintain a specific current density.[60-62] That is, a current is passed through the wafer and siloxane film in plasma anodization.

In Fig 3.14,(the thermally treated sample) the most intense peak is the Si-O-Si stretch (1133cm^{-1}), which shows no significant difference from that

Unit (Anstrom)

	Thickness (Before)	Thickness (After)	Refractive Index
Control	1962	1962	1.566
Thermal	1986	1734	1.556
O_2 plasma floating	1946	425	1.322
Current plasma anodization	1934	494	1.444

Table 3.4 Changes of film thickness and refractive index as a function of different plasma treatments.

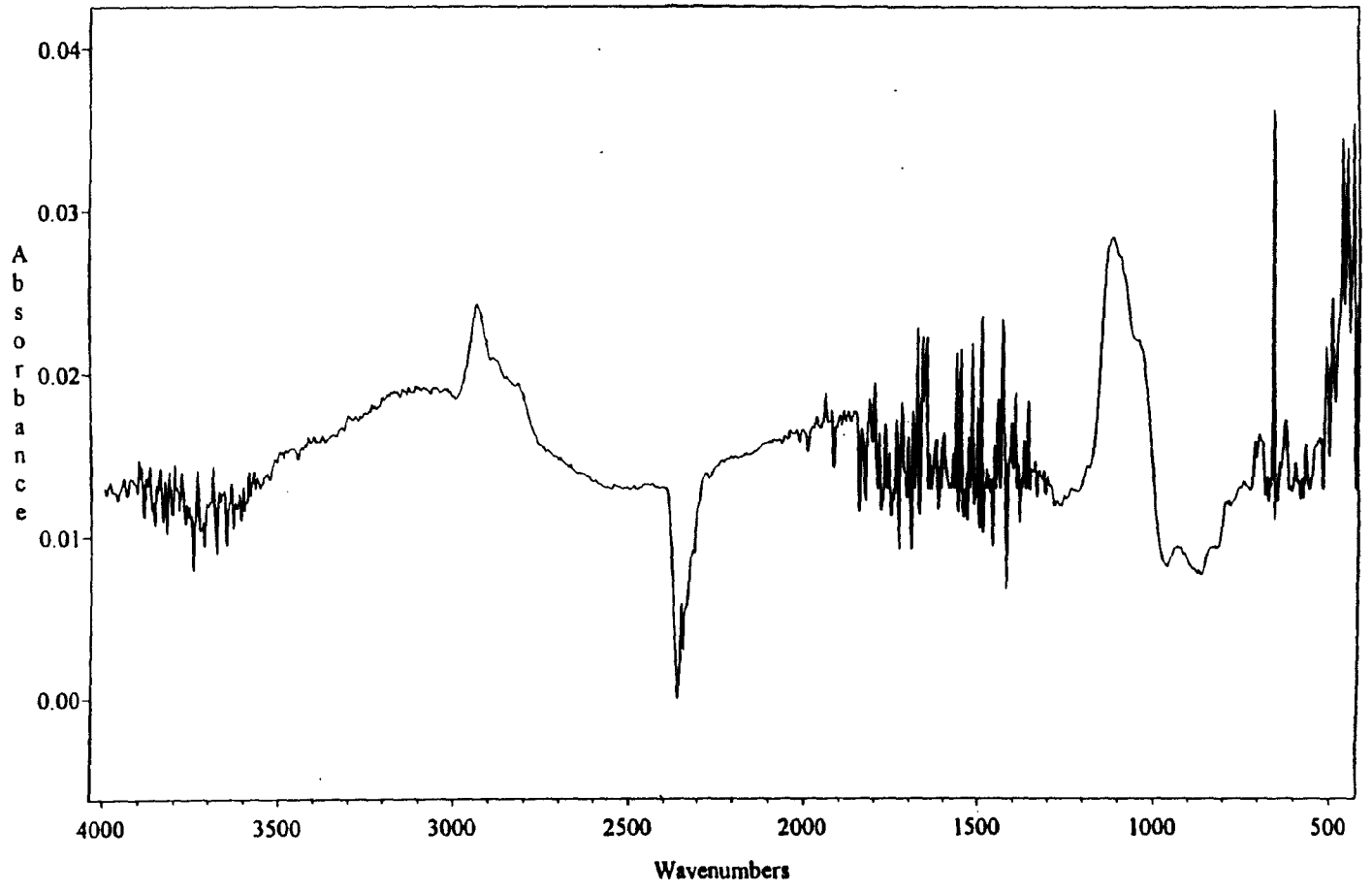

Fig.3.14 FTIR spectrum of an SOG film after treatment in O_2 at 30mTorr, 250^{0}C, for 40 minutes

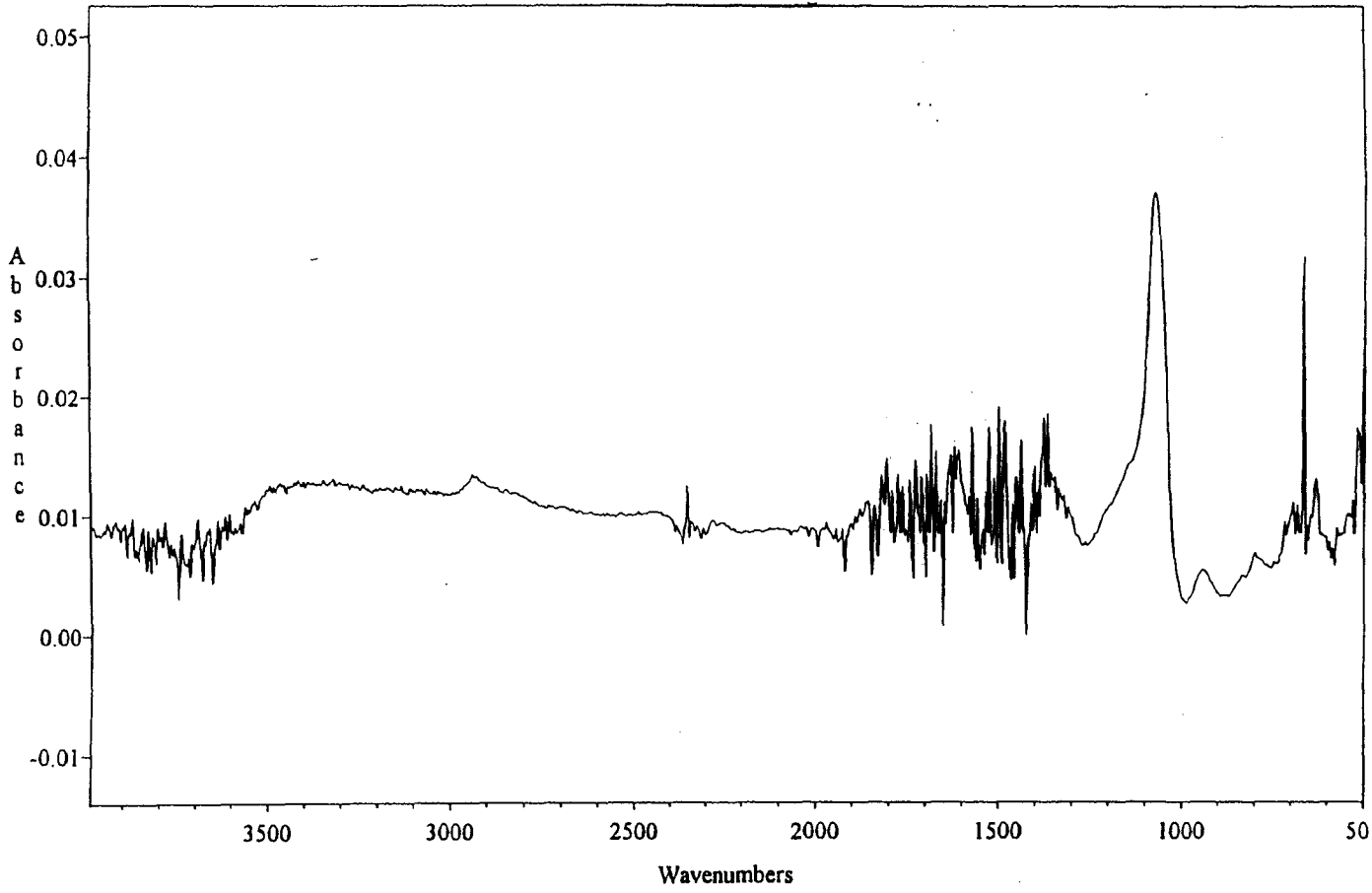

Fig.3.15 FTIR spectrum of O_2 plasma-converted SOG film in substrate floating condition.(30mTorr, 300W, 250^{0}C, for 40 minutes)

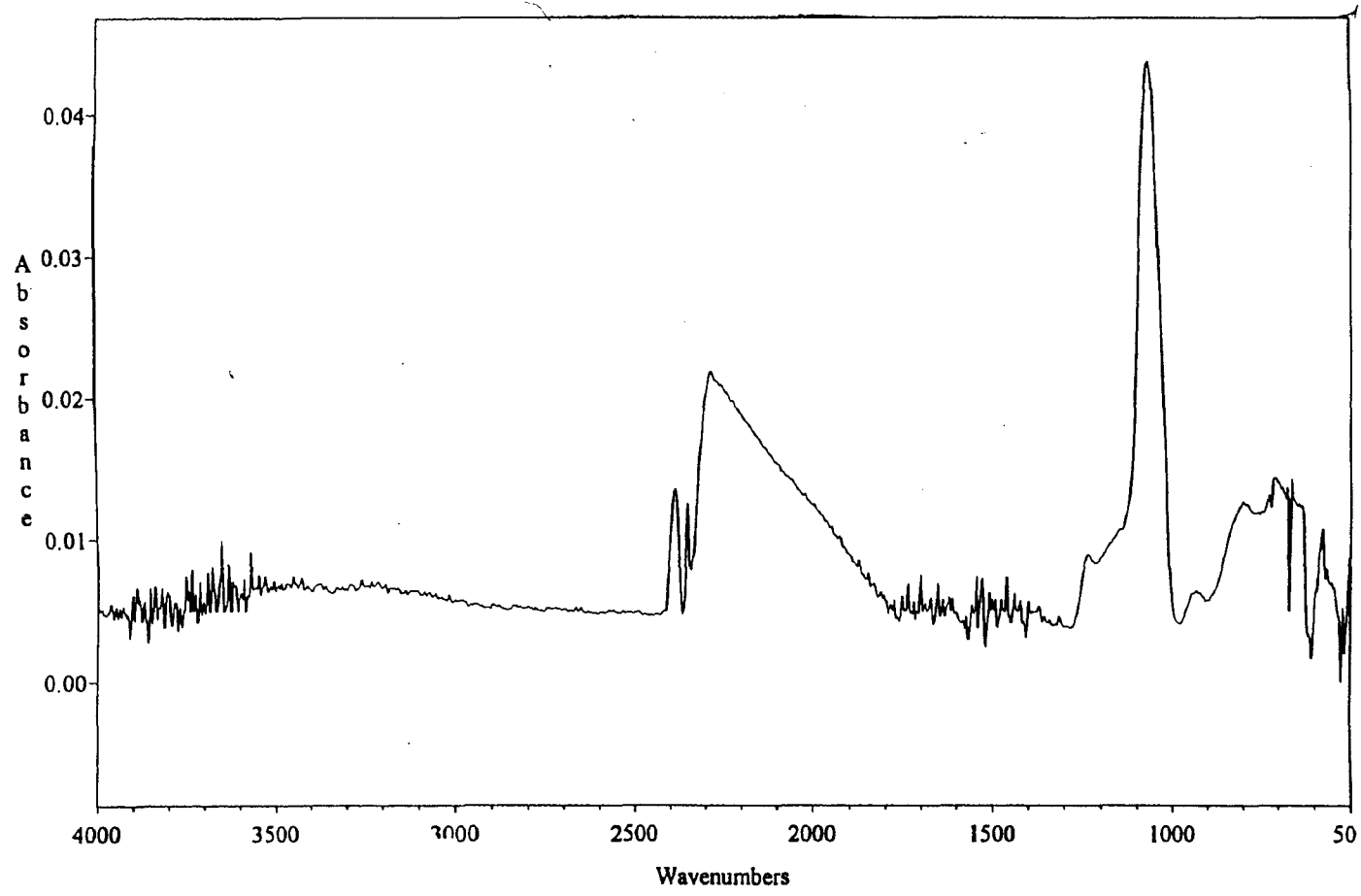

Fig.3.16 FTIR spectrum of O_2 plasma-converted SOG film under plasma anodization conditions. (30mTorr, 300W, 250^{0}C, 40 minutes, current density is 1.78 mamp/cm^2)

of the 200^{0}C or 300^{0}C oxygen annealed sample. (Fig.3.9) The C-H stretching (2936-2836cm^{-1}) vibration did not diminish much in the thermally treated sample. Also, the hydroxyl (O-H) stretching vibration (3200-3700cm^{-1}) is still located at 3450cm^{-1}.

In Fig 3.15, the substrate floating sample, the most intense peak at 1073 cm^{-1}, is the asymmetric Si-O stretching vibration (thermal-like oxides). The C-H stretch (2936-2812 cm^{-1}) was eliminated by substrate floating plasma treatment. In the hydroxyl (O-H) stretching region (3200-3700cm^{-1}), the O-H peak (3450cm^{-1}) shifts to higher wavenumber (3500cm^{-1}) when the 3600cm^{-1} shoulder becomes more apparent. This suggests that the hydrogen bonded silanol has changed into isolated silanol.

In Fig.3.16, the plasma anodized sample, the most intense peak at 1067cm^{-1}, is the asymmetric Si-O stretching vibration (thermal-like oxide). For this sample, essentially no clear features are observed in the C-H (2936-2812cm^{-1}) region or hydroxyl (O-H) region (3200-3700 cm^{-1}) ; this suggests that most of the O-H bonding is removed by plasma anodization. The results in Fig 3.14-3.16 suggest that the substrate floating (or anodization) condition plays a more aggressive role in removing the organic groups, water, or O-H, and in converting polysiloxane into an silicate-like structure throughout the bulk of the spun-on layer.

Table 3.4 shows the change of film thickness and refractive index

before and after different plasma treatments. The original refractive index is ~1.566. After O_2 plasma treatment,, the refractive index decreases to 1.322 and 1.444 in substrate floating and in anodization cases, respectively. In the thermal case, the refractive index stay the same (~1.56), which suggests that low temperature thermal treatment is not an effective way to convert the polysiloxane films into silica-like structures. This is supported by that the following facts: the wavenumber of the dominant peak is not in the thermal oxide region, the C-H stretch (2936-2812cm^{-1}) is not eliminated by this treatment, and the shoulder (3600cm^{-1}) of the O-H stretching (3200-3700cm^{-1}) region is not apparent.

Both substrate floating and anodization cases are effective in removing organic groups in the film and converting the polysiloxane into silica-like glass. The composition changes cause the refractive indices to drop in both cases. A reduction in film thickness is observed for both the floating (~152 nm) and anodization (~144 nm) conditions, while in the thermal case, there is little thickness reduction (~25nm). The oxygen species (atoms, ions) attack the surface and oxidize hydrocarbon components in the film which results in a significant film thickness reduction in the substrate floating and anodization cases. In a comparison of Tables 3.3 and 3.4, the effect of plasma anodization at 250^{0}C is almost the same as to the that of an anneal at 800^{0}C

in oxygen in reducing the film thickness. (thickness decrease ~148 nm). The film thickness after an 800^{0}C oxygen annealing treatment is 48.3 nm while in the plasma anodization case, it is 49.4 nm. In Fig 3.13, the index of refraction for an 800^{0}C oxygen annealed film is ~1.43, which is close to the index of refraction after plasma anodization (~1.44); this suggests that plasma anodization (250^{0}C) has almost the same effect as that of the 800^{0}C thermal anneal with oxygen.

In Table 3.4, the refractive index of the 250^{0}C low pressure case is 1.556, which is close to 1.56 in the 300^{0}C oxygen anneal condition. The two treatments give similar results, it is probably due to the similar temperature, or to the use of low pressure. The refractive index of substrate floating and current plasma anodized film is 1.322 and 1.444, respectively.

3.7. Etching

A. Dry Etching

Fig 3.17 shows the relationship between etch depth in O_2 plasma at 50sccm, 50mTorr, 250W, 35^{0}C for 2 and 5 minutes for SOG samples nitrogen annealed at different temperatures. These results show that the lower temperature nitrogen annealed samples etch faster due to the higher hydrocarbon content of the films. The O_2 reactive species react readily with hydrocarbon species to yield more rapid etch rates. Between 600 and 1000^{0}C,

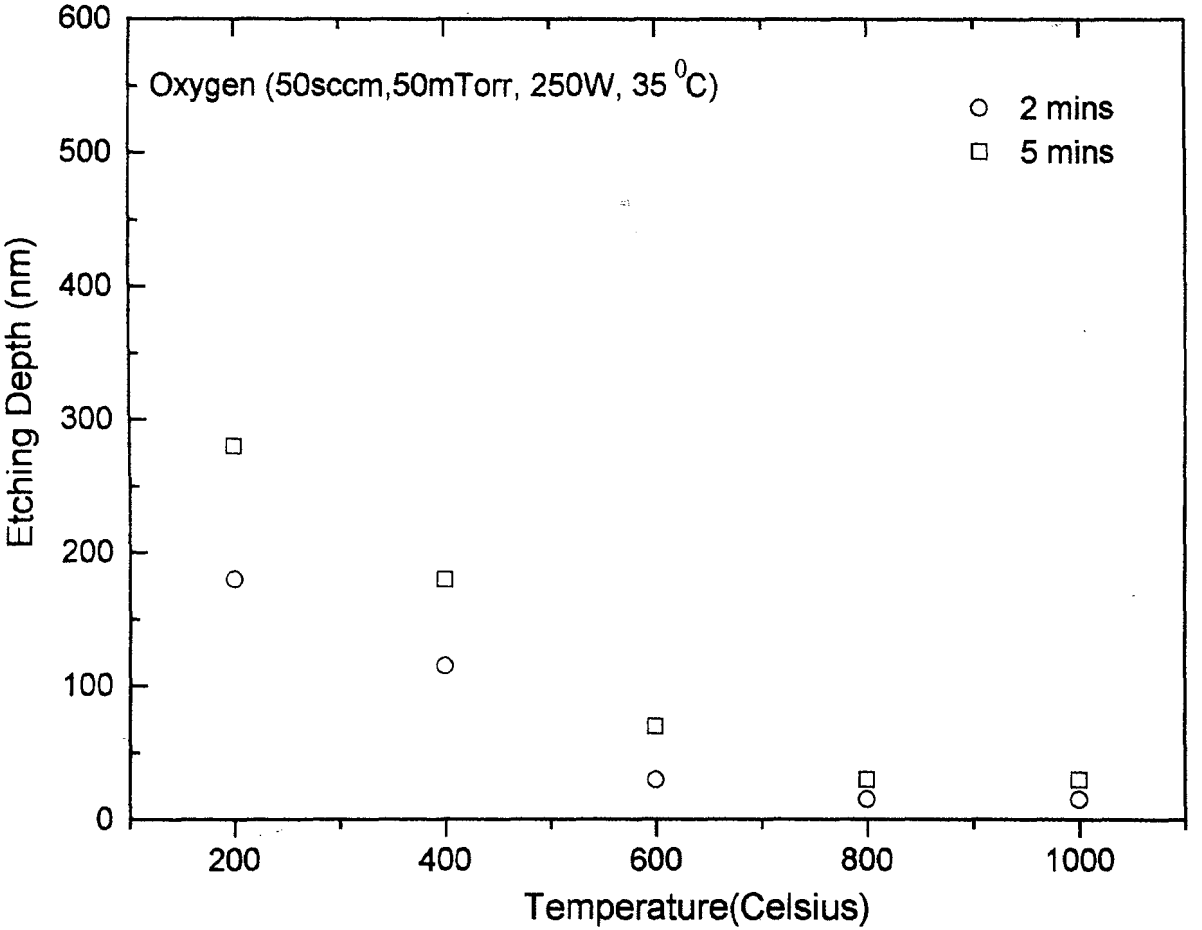

Fig 3.17 Oxygen reactive ion etch depth of samples annealed at temperatures

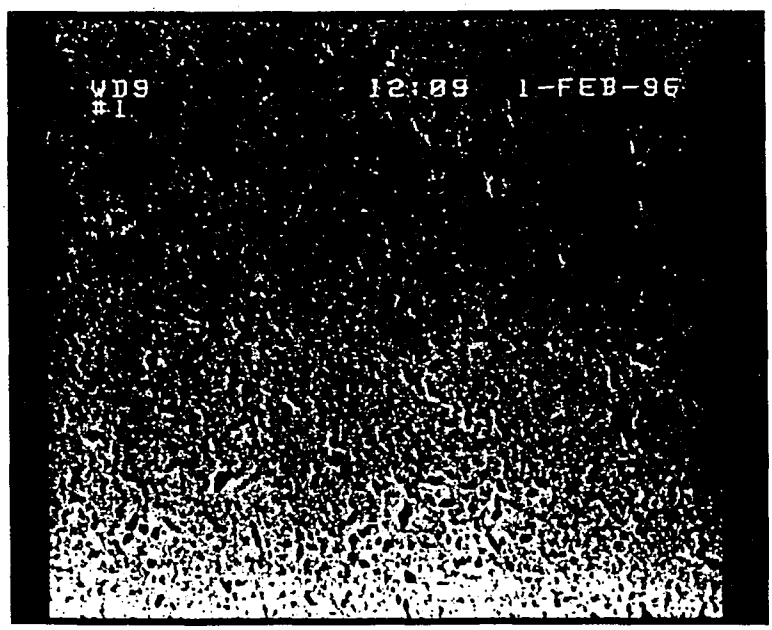

Fig.3.18 SEM picture of 200^{0}C nitrogen annealed sample after O_2 reactive ion etching.(50sccm, 50 mTorr, 250W, 5 minutes)

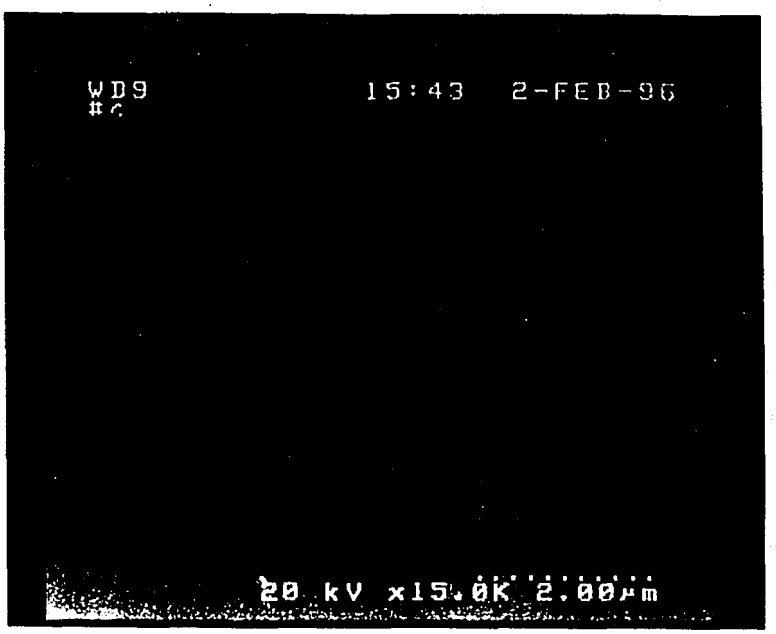

Fig.3.19 SEM picture of 600^{0}C nitrogen annealed sample after O_2 reactive ion etching.(50sccm, 50 mTorr, 250W, 5 minutes)

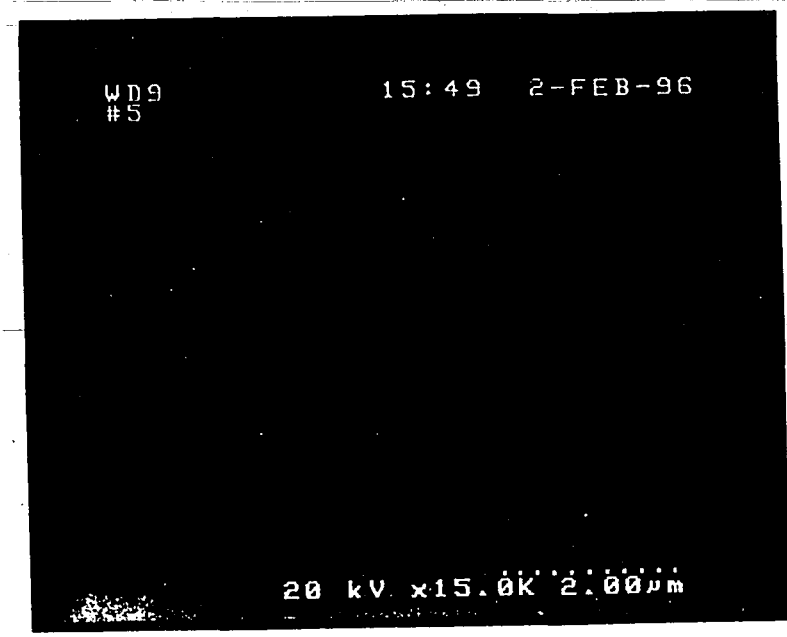

Fig.3.20 SEM picture of 1000^0C nitrogen annealed sample after O_2 reactive ion etching.(50sccm, 50 mTorr, 250W, 5 minutes)

the etch depth for a specific each time continues to drop as a result of glass densification and lower hydrocarbon content. Under these conditions, film (essentially silica) etching is due almost solely to sputtering.

Figs. 3.18 , 3.19, and 3.20 are SEM pictures of 200^{0}C, 600^{0}C, 1000^{0}C nitrogen annealed samples after O_2 reactive ion etching (RIE) (50sccm, 50mTorr, 250W, 35^{0}C, 5 minutes), respectively. Clearly, the morphology of 200^{0}C nitrogen annealed samples after O_2 reactive ion etching shows porosity. However, the SEM pictures of 600^{0}C and 1000^{0}C nitrogen annealed samples have smoother surfaces than the 200^{0}C sample after O_2 reactive ion etching. These pictures confirm why etch depth is higher foe samples with lower temperature anneals. The hydrocarbon content and porosity in the films have a significant effect on the O_2 reactive ion etching process. Above 600^{0}C, glass densification and lower hydrocarbon content result in a smoother surface after O_2 reactive ion etching.

Figs.3.21. and 3.22 show the relationship between SOG samples nitrogen annealed at different temperatures and etch depth in mixtures of (80%CHF_3/20% O_2) and (90% CHF_3/10% O_2), respectively. These etch conditions were: 250Watts, 35^{0}C, 50mTorr and etch times of 5 and 10 minutes. In Fig.3.21, there is no significant difference in etch depth between 200^{0}C and 400^{0}C nitrogen annealed samples. For nitrogen annealed

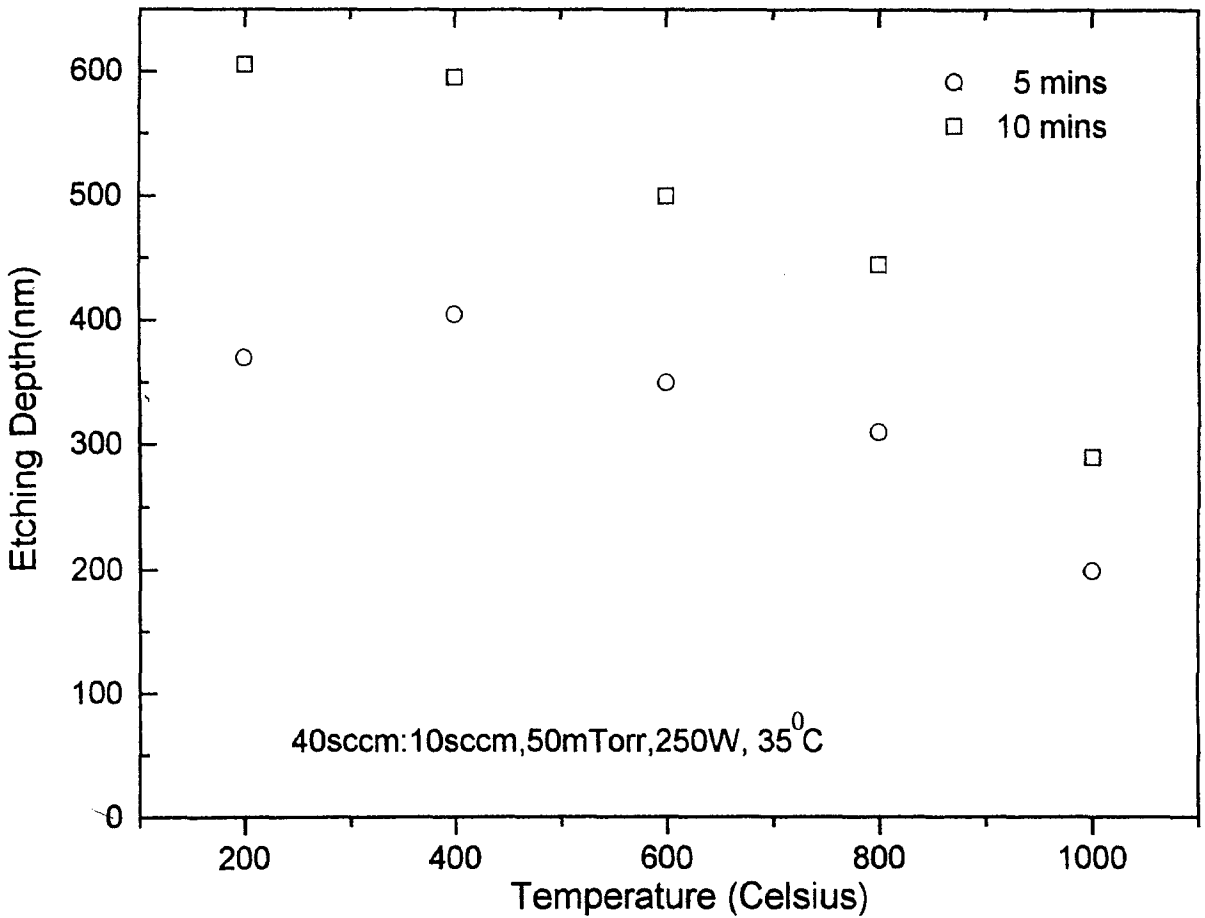

Fig 3.21 Etch depth of nitrogen annealed samples after CHF_3/O_2 (80%:20%) reactive ion etching

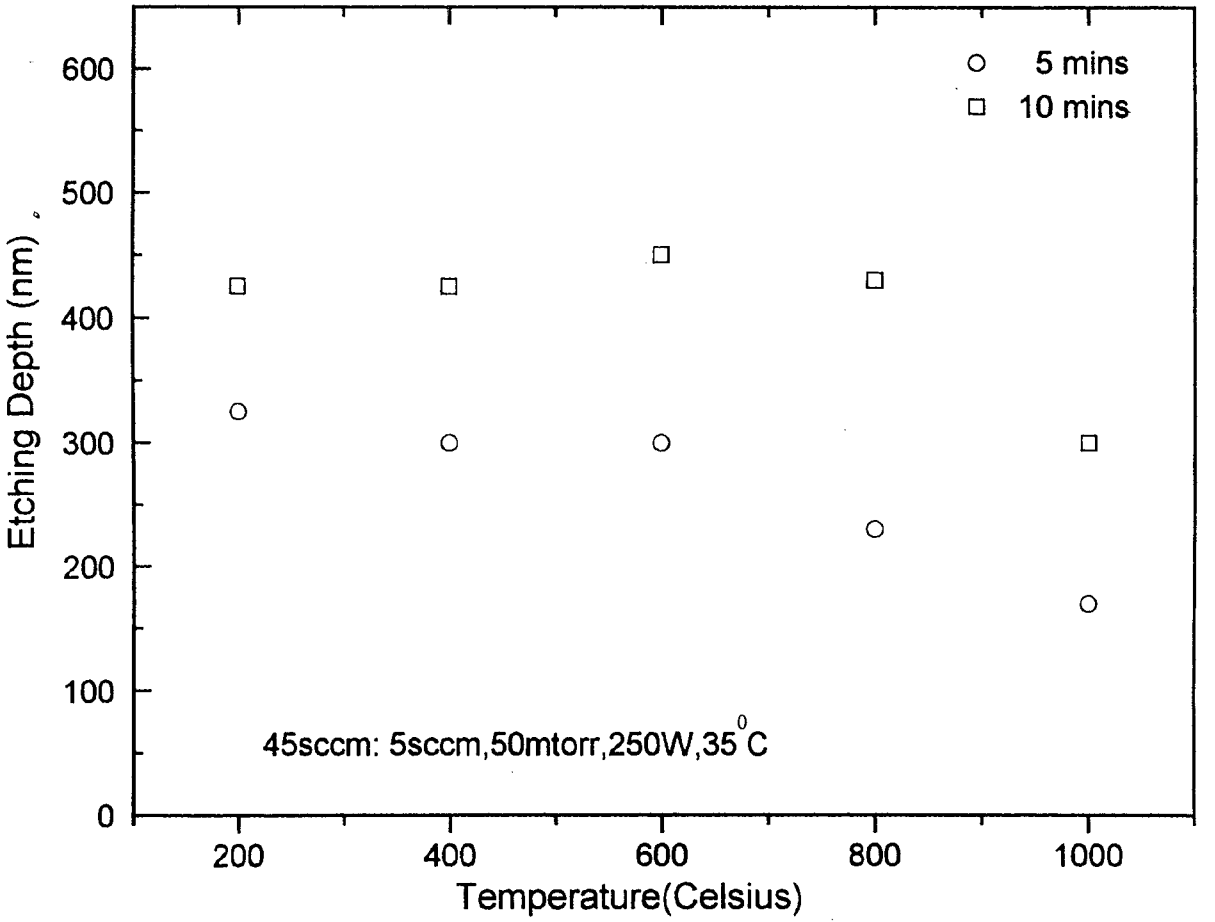

Fig 3.22 Etch depth of nitrogen annealed samples after CHF_3/O_2 (90%:10%) reactive ion etching.

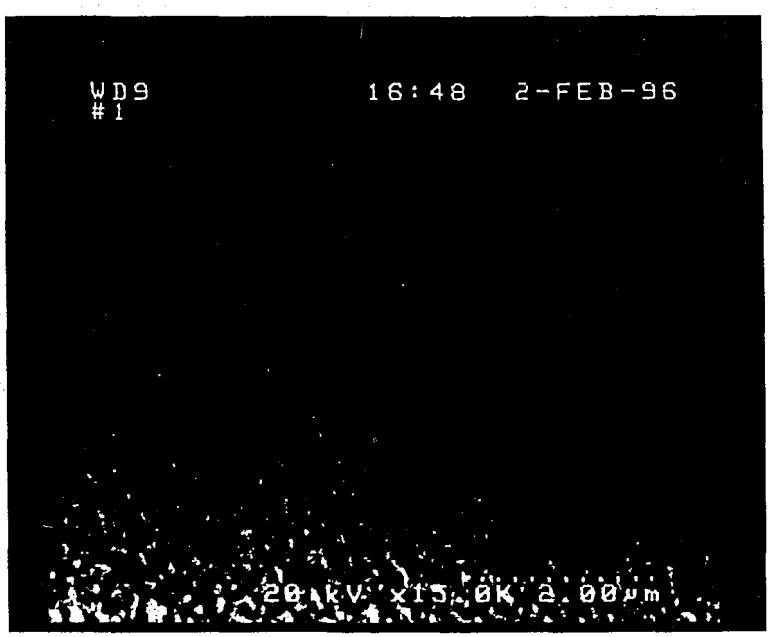

Fig.3.23 SEM picture of 200^{0}C nitrogen annealed sample after CHF_3/O_2 (90%:10%)reactive ion etching.(50 mTorr, 250W, 35^{0}C, 10minutes).

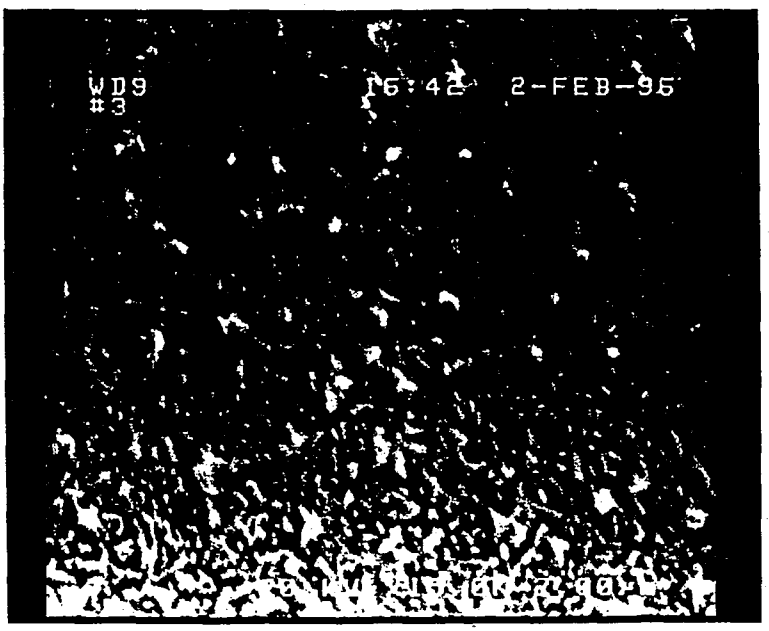

Fig.3.24 SEM picture of 600^{0}C nitrogen annealed sample after CHF_3/O_2 (90%:10%)reactive ion etching.(50 mTorr, 250W, 35^{0}C, 5 minutes).

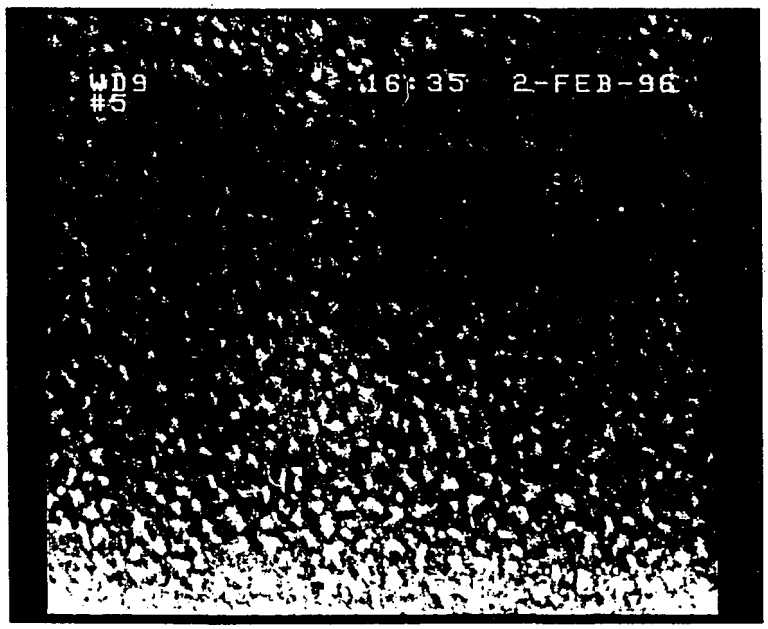

Fig.3.25 SEM picture of 1000^{0}C nitrogen annealed sample after CHF_3/O_2 (90%:10%)reactive ion etching.(50 mTorr, 250W, 35^{0}C, 10 minutes).

samples at temperatures between 600^0C and 1000^0C, the etching depth decreases continuously. These results are due to the highes level of porosity and hydrocarbon content that exists at the lower anneal temperatures. The same general trend is seen in Fig.3.22, for an etch gas mixture of 90% CHF_3 and 10%O_2. However, due to the extensive densification, a significant drop in etching occurs for the sample annealed at 1000^0C. Hoek et al [62] and Mogab et al [63] have demonstrated that oxygen reacts with CF_4 to form CO, CO_2 , and COF_2 by consuming carbon in the mixture gas, and release F to enhance the etching rate oif silicon-containing materials. Increasing oxygen content results in an incrase in the F/C ratio and thus a higher etch rate. Indeed, the etch depth in Fig.3.21 is higher than in Fig.3.22 between 200^0C to 600^0C.

Figs.3.23 ,3.24, 3.25 are SEM pictures of 200^0C, 600^0C, and 1000^0C nitrogen annealed samples after O_2/CHF_3 (10 %: 90 %) reactive ion etching, respectively. These results indicate that under CHF_3/O_2 reactive ion etching the surface is rougher than after O_2 reactive ion etching, because fluorine atoms etch the surface chemically at different rates, depending upon the surface composition.

B. Wet Etching

The main difference between wet etching and dry etching is that wet etching is isotropic while dry etching can give anisotropic profiles.[64]

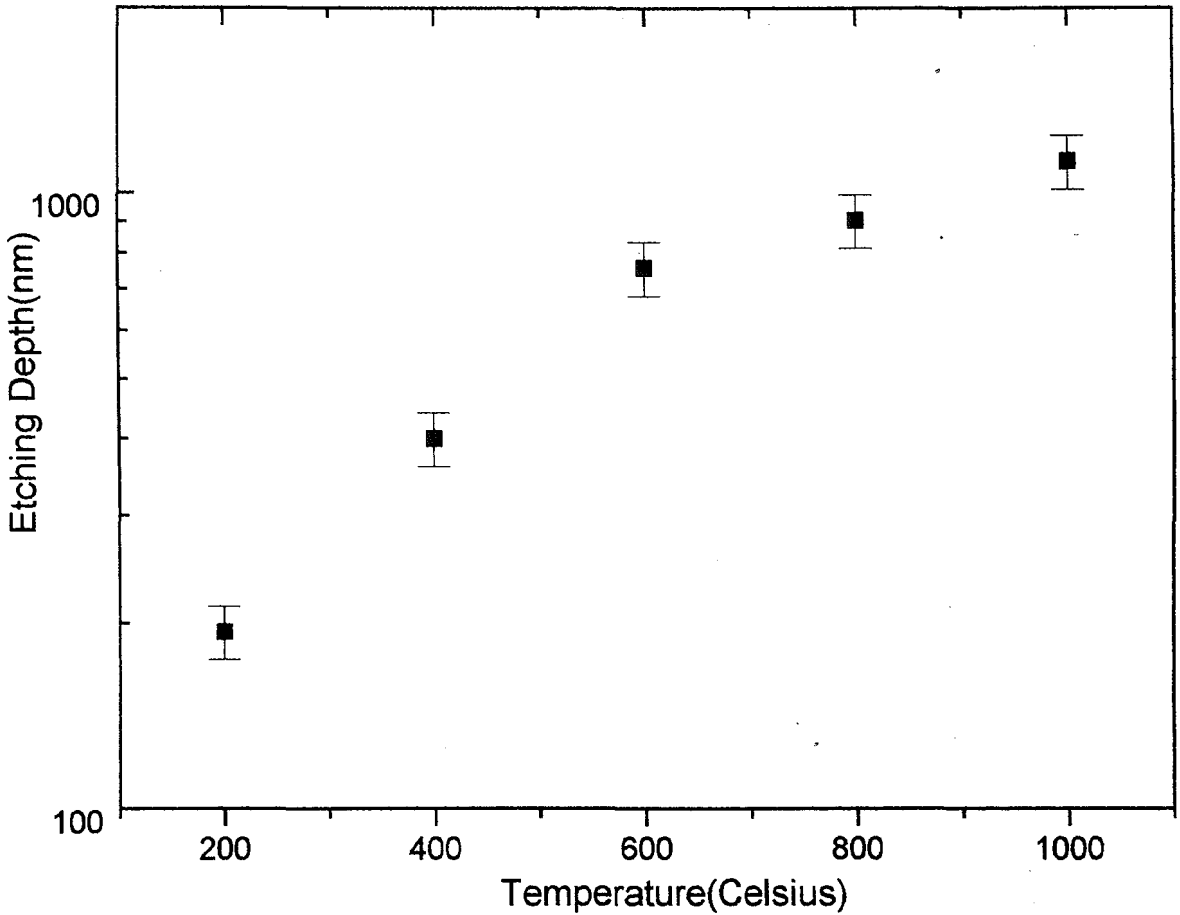

Fig.3.26 Dependence of BHF(HF:NH_4F=1:500) wet etch depth of SOG films on curing temperature after 1 minute of etching

Thus, dry etching is used in devices fabrication, while wet etching is frequently used to assess film density.

Fig.3.26 is the wet etching depth of nitrogen annealed samples in BHF (NH_4F:HF= 500:1) for 1 minute. The chemical reaction for SiO_2 wet etching can be shown as follows [65]:

$$SiO_2 + 6HF \text{ ----------} > H_2SiF_6 + 2H_2O$$

In Fig 3.26, the etching depth of 200^{0}C nitrogen annealed sample is lower than that of a 1000^{0}C annealed sample. Nakano et al.[42,66] have reported that SOG films with higher carbon contents have lower etch rates. The presence of Si-C rather than Si-O-Si bonds results in the lower etching rate. Other studies have shown that the presence of carbon inhibits the etching in buffered oxide etch [67,68] (BOE). This agrees with the results in Fig.3.26 and XPS data, since as the anneal temperature increases, there is less and less carbon and more silicate-like material in the film. Therefore, the highest etching rate in observed for the 1000^{0}C nitrogen annealed sample.

Generally speaking, the wet etching rate can be used as an indicator of the CVD and thermal oxide film quality, but for organic SOG films, this is not necessarily the case.[66,69]

3.8 Electrical Properties

A. C-V Analysis

Dielectric constants of SOG films after nitrogen annealing at 400^0C, 600^0C, and 1000^0C are shown in Table 3.5. The characterization was performed by using capacitance voltage (C-V) characteristics of a metal/insulator/silicon (MIS) capacitor. Table 3.5 shows capacitance, film thickness dot area, and dielectric constant of 400^0C , 600^0C and 1000^0C samples.

Figs.3.27 3.28 are typical C-V plots of samples nitrogen annealed at 400^0C and 600^0C, respectively. As the anneal temperature increases from 400^0C to 600^0C, the type of electrical instability in the films changes. Brooks et al.[70] have deposited Si_3N_4 films by PECVD and showed that when depositing at an R.F power of 25W and below, polarization effects dominate, while at 35 W and above carrier trapping phenomena at the silicon-insulator-metal interface dominate. The comparison here is that the higher temperature can be compared to a higher R.F. power.

As shown in Fig. 3.27, the 400^0C annealed sample exhibits hysteresis, while at 600^0C, trapping dominates. Gazicki et al.[71] and Szeto et al [72] have identified that films which contain substantial amounts of carbon typically exhibit polarization. The trapped carbon and silicon radicals reacts with oxygen species and create polar sites such as hydroxyl and Si-O. This explanation is consistent with the presence of Si-O, and O-H stretches in

	400^0C	600^0C	1000^0C
capacitance	$7.25x10^{-11}$	$3.5x10^{-10}$	$1.26x10^{-10}$
film thickness	96nm	49.8nm	32.1nm
area	$1.25x10^{-3}$ cm^2	$1.25x10^{-3}$ cm^2	$1.25x10^{-3}$ cm^2
dielectric constant	6.28	15.7	3.65

Table 3.5 Capacitance, film thickness , dot area, and dielectric constant of 400^0C, 600^0C and 1000^0C annealed samples under nitrogen ambient.

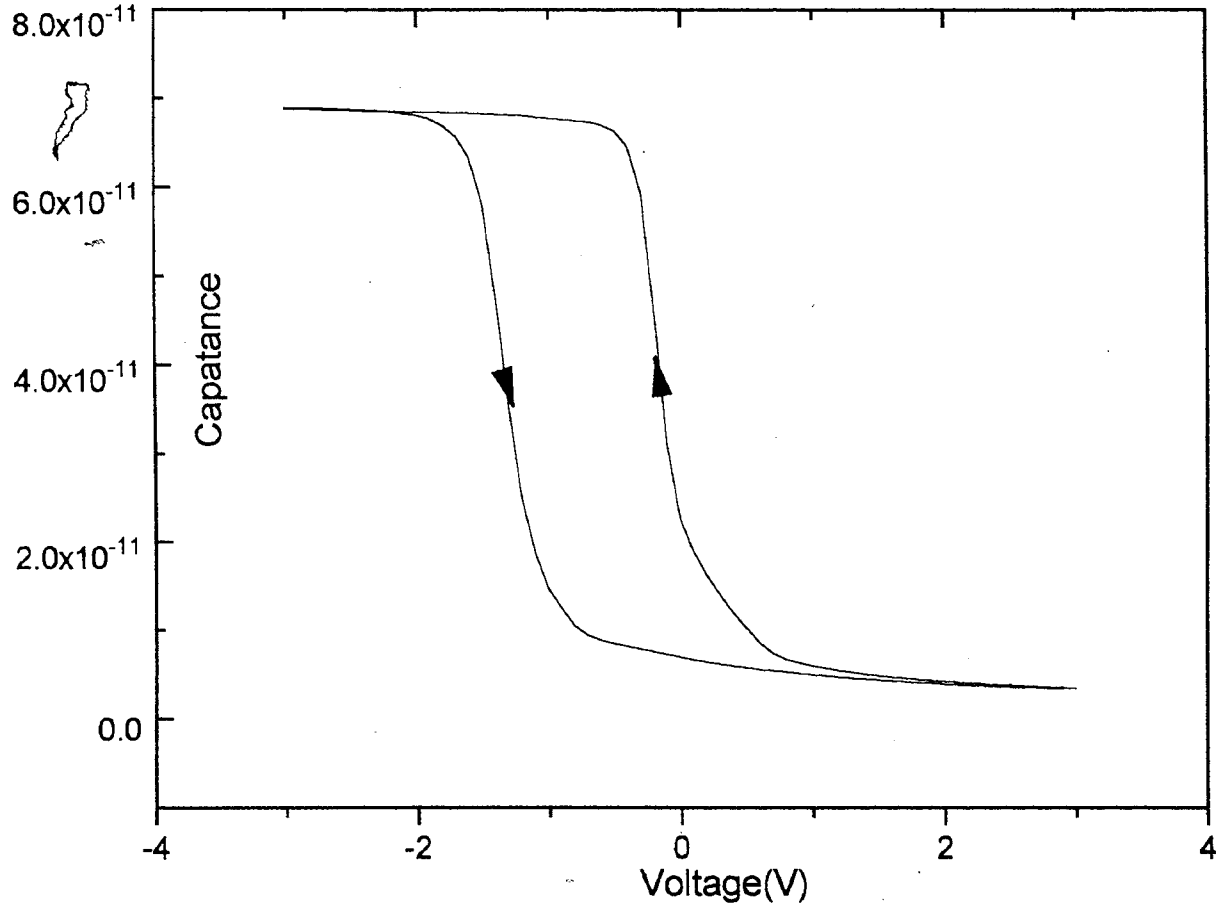

Fig.3.27 Typical CV plot for 96 nm film annealed at 400^{0}C in nitrogen

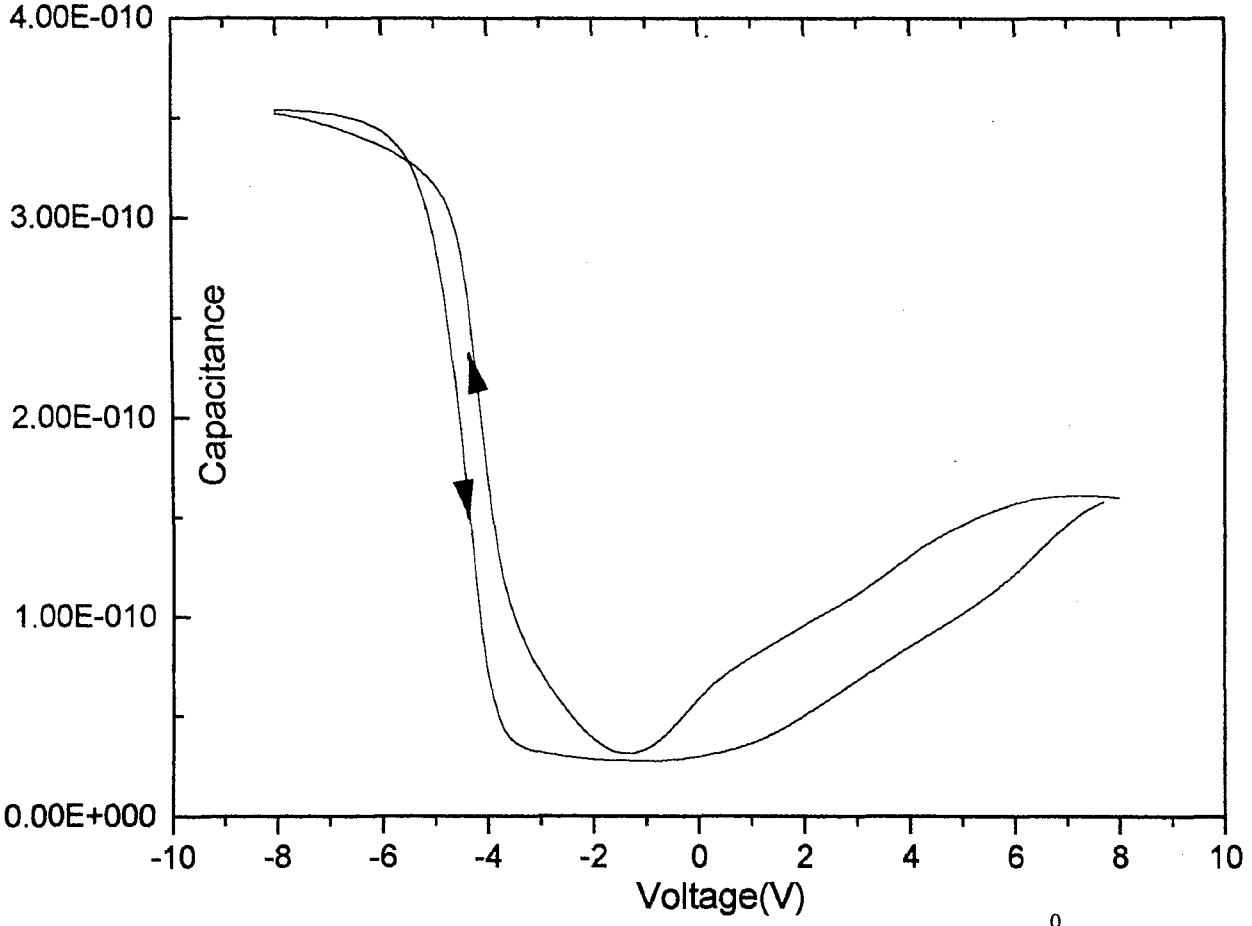

Fig 3.28 Typical CV plot for 49.8 nm film annealed at 600 ^{0}C in nitrogen

the FTIR spectra.

In Fig.3.28, the 600^{0}C nitrogen annealed sample exhibits more negative flat band voltage shift and the hysteresis width becomes narrower, which suggests the a positive charge trapping instability. A possible reason is that 600^{0}C annealed polysiloxane films with lower carbon content (C/Si<1) are produced at this temperature or above. In addition, refractive index might be used as an indicator of electrical instability. In Fig.3.13, the refractive index is 1.43-1.46 between 600^{0}C and 1000^{0}C . This suggests that annealed polysiloxane films with relatively low carbon content are produced at or above 600^{0}C. A possible reason why the dielectric constant of 400^{0}C annealed film is lower than that of the 600^{0}C nitrogen annealed sample may be the substitution of Si-C and Si-O-Si bonding in 400^{0}C for highly polarized Si-O, as shown in the FTIR spectra.(Fig.3.4-3.9)
Another likely reason maybe due to the large adsorption from carbon radical or dangling silicon which absorb water and have more contribution in increasing the dielectric constant.

Generally speaking, the dielectric constant of SOG films usually decreases as the organic content increases and the water contents decreases. The dielectric constant of 1000^{0}C nitrogen annealed sample is 3.43 which is close to thermal oxides with a dielectric constant of 3.9. The reason why the

dielectric is lower than 3.9 may be due to two reasons. the first reason is that the 13% carbon still left on the film at 1000^0C, thus, the dielectric constant is lower than 3.9. Another likely reason is because of the deficiency of oxygen at the oxidation, suboxide and defects form in the film which decrease the dielectric constant.

B. I-V Analysis

Figs. 3.29. 3.30 are the current density (J) vs. electrical field (E) plots of samples annealed at 400^0C and 600^0C, respectively. The film thickness is 96 nm for 400^0C annealed film and 49.8 nm for 600^0C annealed film, respectively. The dielectric strength of the 600^0C annealed film is approximately 1 MV/cm^2 (measured at 0.1 micro amp/cm^2), while the dielectric strength of the 400^0C annealed film is greater than 1 MV/cm^2. Gina[73] has deposited silicon oxycarbide films from hexamethylcyclotrisiloxane (HMCTS). This results shows that films deposited at high discharge powers (>0.66 W/cm^2) also have low dielectric strength. Here, the higher rf power also can be compared to higher annealed temperatures.

The lower dielectric strength of 600^0C nitrogen annealed films is possibly related to the their large "dangling bond" densities, which result in more conductive films. The higher annealed temperature provides higher energy, and the Si-CH_2 bond in the backbone can be broken easily. Thus, Si

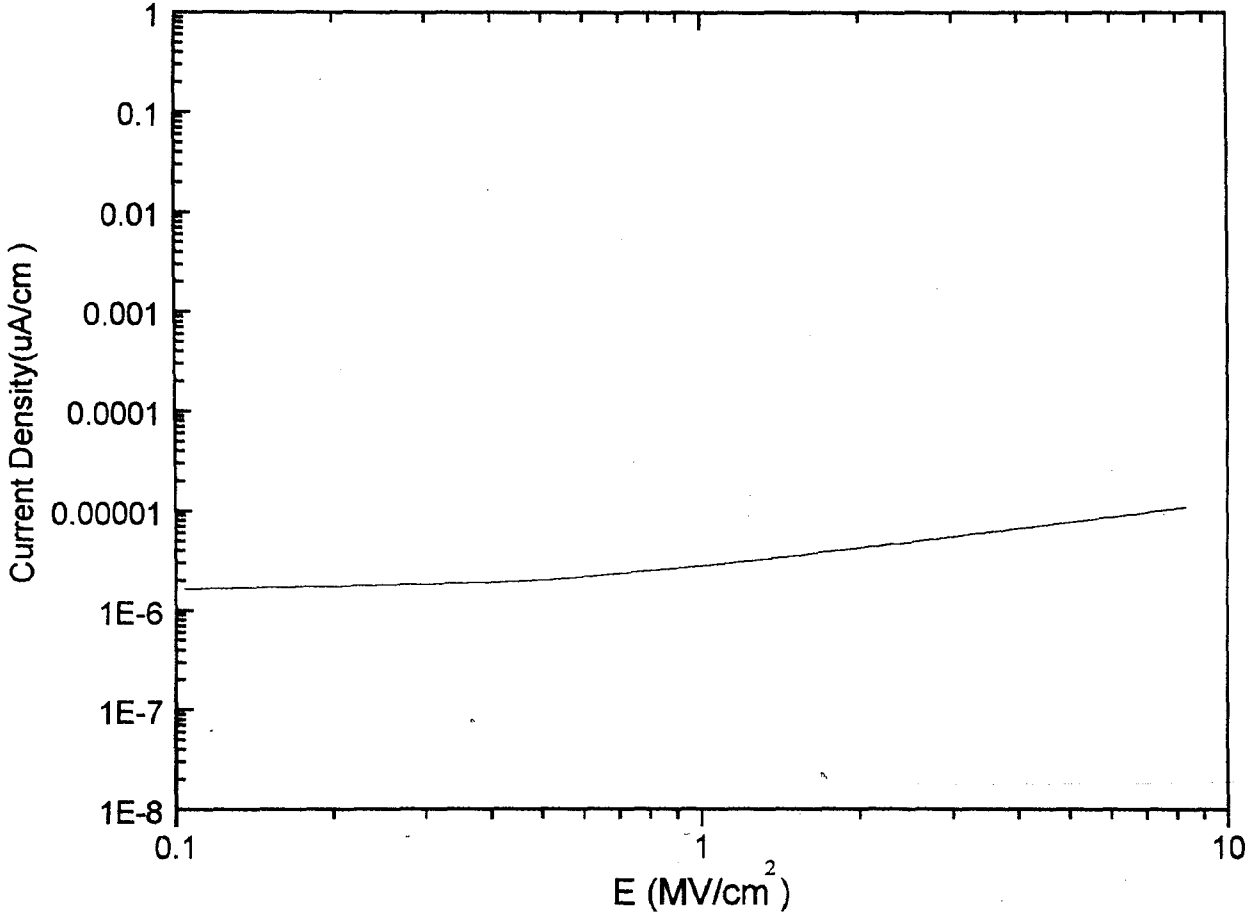

Fig3.29 Current density (J) versus electrical field (E) for 96nm film at 400℃ in nitrogen

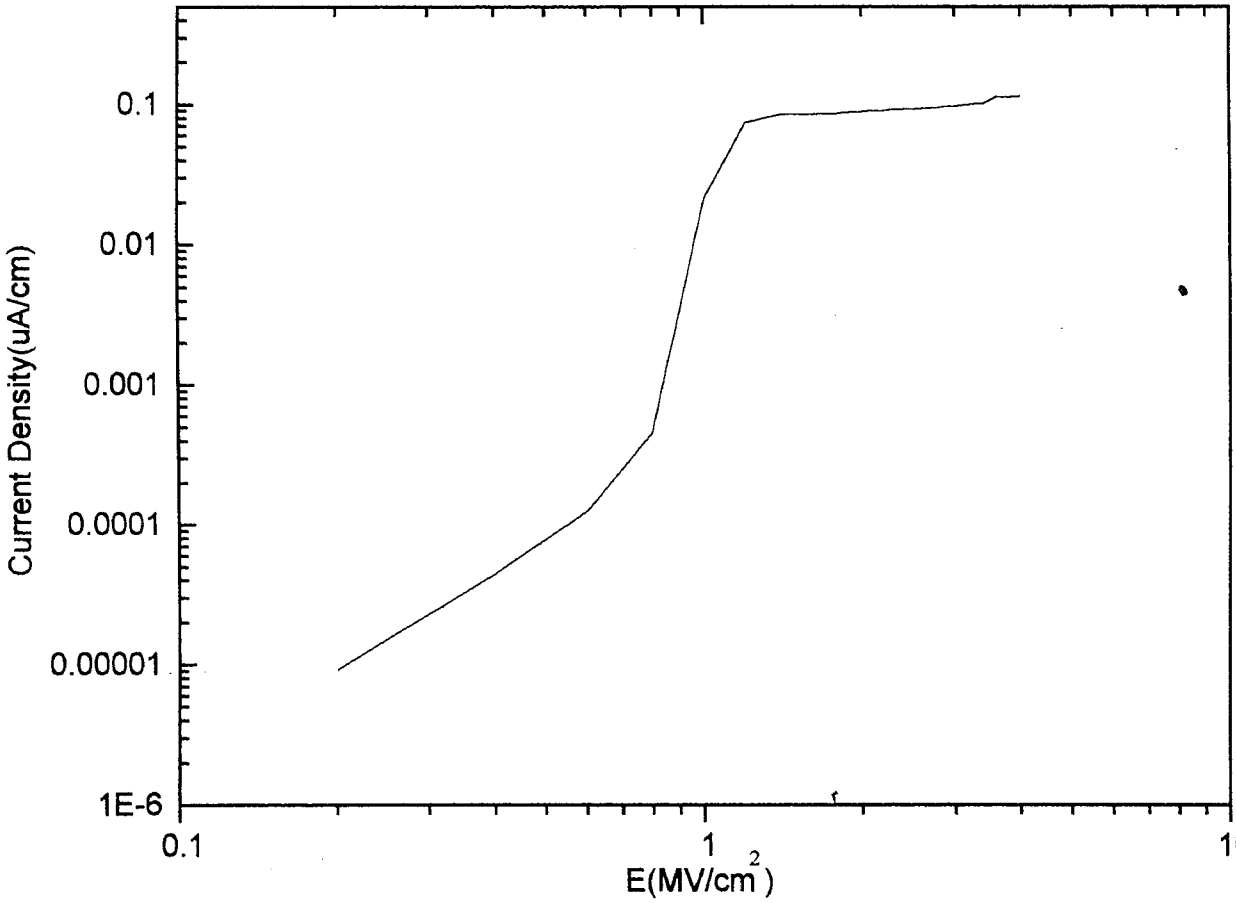

Fig.3.30 Current density (J)versus electrical field (E) for 49.8 nm film at 600^{0} C in nitrogen

dangling bonds can form after CH_2 is removed. The dangling bond acts as the electron hopping site to increase the conduction. Other study has identified that the conduction increases as a result of an increase in spin density.[74] In fact, spin density increases due to a decrease in C-H bonding. The C-H incorporation decreases as the temperature increases from 400^0C to 600^0C. This is shown in the XPS data and FTIR spectra. Thus, the 600^0C annealed films have large spin density and this leads to low dielectric strengths and enhanced conductivity.

Chapter 4

Summary and Conclusion

The effect of different anneal temperatures and ambients on the composition of SOG films have been evaluated in this study. Films properties are strongly related to the organic content. It is concluded that refractive index, film shrinkage, wet etching rate, dry etching rate, and dielectric constant are dominated by the organic content of the SOG. From the analytical techniques used in this study, glass densification occurs at ~600^{0}C for all annealing ambients. XPS data confirm these finding and shows that the organic content decreases at higher annealing temperatures.

After 400^{0}C anneals , the Si-O-Si symmetric stretching vibration gradually converts into an asymmetric Si-O stretch. This is due to the Si-O-Si forms a adsorption site to adsorb water and result in a bonding environment change. The bonding environment changes from hydrogen bonding silanol (or hydrogen -bonded water)change into isolated silanol. And the he isolated silanol can be s eliminated at temperature of 800^{0}C. After 800^{0}C, the oxidation occurs in all annealing ambients except in nitrogen. This can be supported by the fact that the continual film shrinkage after 800^{0}C in nitrogen anneal.

Oxygen plasma-conversion of SOG films is an effective method of

removing organic groups from the films at a low temperature (250^{0}C). At this temperature, SOG films can be converted into silicate-like glass films which exhibit similar chemical structures and characteristics of CVD deposited SiO_2 and thermal oxides by substrate floating and anodization treatments.

The dielectric constant of SOG films can be attributed to the amount of silanol, water, and organic content in the films. Usually, a higher amount of water and silanol will yield a higher dielectric constant.

In this study, to conversion of organic SOG material into silicate-like materials by heating requires temperatures above 800^{0}C. Unfortunately, this is above the temperature that aluminum metallization can tolerate in silicon integrated circuits (ICs). O_2 plasma exposure can be an effective way to get obtain silicate like material from SOG at low temperature.

As a result of different carbon content at various temperatures which influences the electron instability. At 400^{0}C, the higher ratio of C/Si leads to polarization in C-V analysis. However, electron trapping phenomenon appears at 600^{0}C result in the films with less carbon content. The 600^{0}C nitrogen annealed films are more conductive than 400^{0}C films. The dielectric strength of 400^{0}C annealed films are larger than 600^{0}C films.

References

1. Th Von Karman, Z. Agnew, *Math. Mech.*, 1233 (1921).

2. A.G. Emsile, F. T. Bonner, and L. G. Peck, *J. Appl. Phys.* **29**, 858 (1958).

3. A. Acrivos, M. J. Shah, and E. E. Petersen, *J. Appl. Phys.* **31**, 963 (1960).

4. W. W. Flack, D. S. Soong, A. T. Bell, and D. W. Hess. *J. Appl. Phys.* **56**, 1199 (1984).

5. L. K. White, in *Advance in Resist Technology and Processing* II, 539, 29, SPIE. (1985).

6. R. H. Wilson and P. A. Piacenta, *J. Electrochem. Soc.*, **133**., 981 (1986).

7. D. E. Bornside, Ph.D. *Thesis*, University of Minnesota, Minneapolis, MN (1988).

8. D. E. Bornside, *J. Electrochem. Soc.*, **137**., 2589 (1990).

9. D. E. Bornside, *Appl. Phys. Lett*, **58**, 1181 (1991).

10. L. E. Stillwagon and R. G. Laarson, *Phys. Fluids A***2**, 1937 (1990).

11. D. B LAVergne and D. C. Hofer, in *Advance in Resist Technology and Processing* II, 539, 115, SPIE.(1985).

12. P. C. Sukanek., *J. Electrochem. Soc.*, ***136***., 3019 (1989).

13. J. Gu, M. D. Bullwinkel. and G. A. Campbell. *J. Electrochem. Soc.*, ***142***., 909 (1995).

14. W. J. Daughton, P. O'Hagan, and F. L. Givens, *Proceeding of the Kodak Seminar on Microelectronics*, G-49, 15 (1978).

15. W. J. Daughton, and F. L. Givens, *J. Electrochem. Soc.*, **129**. 173 (1982).

16. G. F. Daman, Proceeding of the *Kodak seminar on Microminiaturization*, **34**, 195 (1969).

17. P. O'Hagan, and W. J. Daughton, in *Proceeding of the Kodak seminar on Microelectronics*, G-48, 95 (1977).

18. H. Kotani, M. Matsurra, A. Fujii, G. Genjou, and S. Nagao, *IEEE IEDM TECH. Dig.* 669 (1989).

19. K.Fujino, Y.Nishimoto, N. Tokumasu, and K.Maeda, *J. Electrochem. Soc.* **138**. 550 (1991).

20. K.Fujino, Y.Nishimoto, N. Tokumasu, and K. Maeda in Proceedings of *1991 IEEE VLSI Multilevel Interconnection Conference*, p 445, Santa Clara, CA, IEEE (1991).

21. K. Machida and H. Oikawa, *J. Vac. Sci. Technol, B4*, 818 (1986).

22. C. H. Ting, H.Y. Lin, P. L. Pai, and W. G. Oldham, *ibid.*, p 61 (1987).

23. F. Whitwer, T. Davies, and C. L. Lage, *ibid.*, pp96-102 (1989).

24. P. Pai, A. Chetty, R. Roat, N. Cox, and C. Ting, *J. Electrochem. Soc.*, **134**. 2829 (1987).

25. C. Chiang and D. B. Fraser. *VMIC*, 397 (1989).

26.S. K. Gupta, Mat. res. Soc. Symp. Proc. Vol **108,** 275 (1988)

27. C. Y. Ting, V. J. Vivalda, and H. G. Schaefer, *J. Vac. Sci. Technol.* **15**, 1105 (1978).

28. D. W. Hess. *J. Vac. Sci. Technol. A2*, 244 (1984).

29. M. A.Hartney, D. W. Hess, and D.S. Soane, *J. Vac. Sci. Technol. B7*, 1 (1989).

30. C. F. Zarowin, *J. Electrochem. Soc., 130*.1144 (1983).

31. N. Moriya, Y. S. Diamond, and Rr. Kalish, *J. Electrochem. Soc.*, **140**. 1442 (1993).

32. B. Chapman, *Glow Discharge Processes*, John Wiley and Sons (1980).

33. Bell, A. T. *Techniques and Application of Plasma chemistry*; Hollahan, J. R; Bell, A. T. Eds.; Wiley: New York, p1 (1974)

34. T. W. Hou. C. J. Mogab, and R. S. Wagner, *J. Vac. Sci. Technol.* ***A*1**, 1801 (1985).

35. A. D. Butherus, T. W. Hou. C. J. Mogab, and H. Schonhorn, *J. Vac. Sci. Technol.* ***B*3**, 1352 (1985).

36. Y .S. Diamand and Y. Nachumovsky, *J. Electrochem. Soc..**137***. 190, (1990).

37. This work was done by Sita. R. Kaluri.

38. P. Gise and R. Blanchand, *Modern Semiconductor Fabrication Technology*, Ch3, Prentice-Hall (1986).

39. D. Meyerhofer, *J. Appl. Phys.*, **49**, 3993 (1078).

40. A. L. Smith. *Spectrochemica Acta,* **16**, 87 (1960).

41. W. O. George, *"Infrared Spectroscopy,"* p189, John Wiley and Sons, New York (1979).

42. T. Nakano, K. Tokunaga, and T. Ohta, *J. Electrochem. Soc.*, **142**. 1303 (1995).

43. H. G. Tompkins and P. W. Deal., *J. Vac. Sci. Technol.* ***B*11**, 727, (1993).

44. B. E. Deal, E. H. Snow, and C. A. Mead, ," *J. Phys. Chem. Solids,* **127**, 1837 (1966).

45. J. Wong and C.A. Angell, *"Glass Structure by Spectroscopy,"* p521, Marcel Dekker, Inc., New York (1976).

46. W. A. Pliskin, *J. Vac. Sci. Technol.* **14**.1064 (1977).

47. M. P. Woo, J. L. Cain, and C. O. Lee, *J. Electrochem. Soc.*, **137**, 196 (1990)

48. D. L. Wood and E. M. Rabinovich, *J. Non-Crystalline Solids* **82**, 171 (1982).

49. D. L. Wood., E. M. Rabinovich, D. W. Johnson, Jr. J. B.MacChesney, and E. M..Vogal, *J. Am. Ceramic Soc.* **66**, 693 (1983).

50. J. A. Thiel, D. V. Hsu, and G. Lucovsky, *J. Electron. Mater.* **19**, 209 (1990).

51. J. A. Thiel, D. V. Hsu, M. W. Watkins, S. S. Kim and G. Lucovsky, *J Vac. Sci. Technol.* ***A*8**, 1374 (1990).

52. H. G. Tompkins and C.Tracy., *J. Vac. Sci. Technol.* **B8**, 558 (1990).

53. M. Nakamura, R. Kanzawa, and K. Sakai, *J. Electrochem. Soc.* **33**, 1167 (1986).

54. B. Bhushan, S. P. Muraka, and J. Gerlach, *J. Vac. Sci. Technol.* ***B*8**, 558 (1990).

55. S. Kern, *RCA. Rev.* **37**, 55 (1976).

56. S. Gourrier and M. Bacal, *Plas. Chem. and Plas. Proc.* **1**, 217 (1981).

57. A. Reisman, in Semiconductor Silicon 1986, *The Electrochemical Society,* Pennington, New York, Vol.86-4, 364 (1986).

58. J. F. O'Hanlon, in *Oxides and Oxide Films,* ed, A. K. Vijh, Marcel Dekker, Inc. New York and Basel, Vol.5, 105 (1977).

59. S. Kimura, E Murakami, K. Miyake, T. Warabisaka, H. Sunami and T. Tokuyama, *J. Electrochem. Soc.* **132**, 1460 (1985).

60. A. Kiermasz, w. Eccleston, and J.L. Motuzzi, *Solid State Electronics* **26**, 1167 (1983).

61. A. J. Van Roosmalen, J.A.G.Raggerm, and S.J.H.Brader, *Dry Etching for VLSI* , Plenum Press (1992).

62. W. G. M. van den Hoek, wt al., *J. Vac Sci. Technol.* **16**. 391 (1979).

63. C. J. Mogab. A.C. Adams. and D.L. Flamm, *J. Appl. Phys.* **49**, 3796 (1983).

64. E. C. Douglas, *Solid State Technology,* **24**, 65 (1981).

65. S. Wolf, *Silicon Processing for the VLSI,* **1**. Ch15, Lattice Press, (1986).

66. T. Nakano and T. Ohta, *J. Electrochem. Soc.,* **142**. 918 (1995).

67. J. Janca, M. Necasova, T. Sikola, *Acta Phys. Slov., 33*. 187 (1983).

68. V. I. Belyi, T. P.Smirnova, A. P, Solovev, I. L. Yasjkin, L. V. Khramova, and I. I. Marakhovka, *Mikroelectronica (Akad. Nauk SSSR), 15*, 146 (1986).

69. S. M. Sze, in *VlSI Technology*, 2nd ed , p157, McGraw-Hill , Inc. New York. (1988).

70. T. A. Brooks.and D. W. Hess, *Thin Solid Films,* **153**, 521 (1987).

71. M. Gazichi, H. Yasuda, *Plasma Chemistry and Plasma Processing, 3*, 279 (1983).

72. R. Szeto, and D. W. Hess, *J. Appl. Phys.,* **52**, 903 (1981).

73. G. M. Buccellato, Ph.D. *Thesis*, University of Califoria, Berkley, CA. (1992)

74. S. Yokayama, M. Hirose, and Y, Osaka, Jpn. *J. Appl. Phys , 20*. L35 (1981)

Vita

Hsiu-Hung Kuo was born in Tainan, Taiwan. R.O.C. on Feb.1968 to P. Y. Kuo and C. S. Chung. he received a B.S in Materials Science on May.1991. After that, he went to military service for two years and came to U.S.A. at August,1994. He began his research under Dr.Hess and Dr.Chaudhury on Jan.1995 and finish at May, 1996. After his graduation, he hope he can devoted himself in manufacturing semiconductor industry.

END OF TITLE